CHALMERS
UNIVERSITY OF TECHNOLOGY

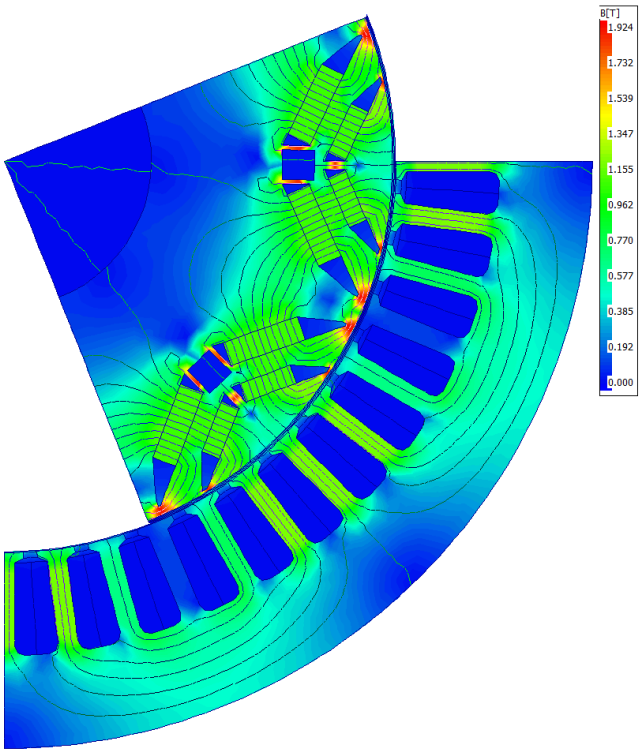

Design parameter optimization of Electric Drive Units

A regression based optimization of PMSM geometrical design parameters and final drive ratio

Master's thesis in Mobility Engineering

ADITHYA RAM PANYAM
CHANAKYA PANGULURU

DEPARTMENT OF MECHANICS AND MARITIME SCIENCES

CHALMERS UNIVERSITY OF TECHNOLOGY
Gothenburg, Sweden 2023
www.chalmers.se

Master's thesis 2023

Design parameter optimization of Electric Drive Units

A regression based optimization of PMSM geometrical design parameters and final drive ratio

Adithya Ram Panyam
Chanakya Panguluru

CHALMERS
UNIVERSITY OF TECHNOLOGY

Department of Mechanics and Maritime Sciences
Mobility Engineering
Chalmers University of Technology
Gothenburg, Sweden 2023

Design parameter optimization of Electric Drive Units
A regression based optimization of PMSM geometrical design parameters, and final drive ratio
ADITHYA RAM PANYAM, CHANAKYA PANGULURU

© ADITHYA RAM PANYAM, CHANAKYA PANGULURU, 2023.

Supervisor: Dhinesh V Velmurugan, Aurobay & Duc-Khanh Nguyen, Aurobay
Examiner: David Sedarsky, Department of Mechanics and Maritime Sciences

Master's Thesis 2023
Department of Mechanics and Maritime Sciences
Division of Energy Conversion and Propulsion Systems
Chalmers University of Technology
SE-412 96 Gothenburg
Telephone +46 31 772 1000

Cover: FEA simulation in Motor-CAD showing cross-sectional view of PMSM.

Typeset in LaTeX
Printed by Chalmers Reproservice
Gothenburg, Sweden 2023

Design parameter optimization of Electric Drive Units
A regression based optimization of PMSM geometrical design parameters and final drive ratio
Master's thesis in Mobility Engineering
ADITHYA RAM PANYAM, CHANAKYA PANGULURU
Department of Mechanics and Maritime Sciences
Division of Energy Conversion and Propulsion Systems
Chalmers University of Technology

Abstract

Permanent magnet synchronous machines (PMSM) are widely used for propulsion system in electric vehicles due to their high efficiency, high torque density, excellent dynamic response and control, and reliability. Significant investments are being made to fund research on improving their efficiency, torque capabilities to enhance overall vehicle performance and driving range. To appropriately determine the size and specifications of the motor for a specific powertrain requirement, numerous geometric, electric, and mechanical parameters need to be considered. In this study, we present a method to optimize certain selected design parameters of the PMSM to improve the performance of the powertrain. The focus of this study is on the geometrical design parameters of the PMSM, while also considering the final drive ratio, to imrprove the performance of the overall powertrain. By employing orthogonal design of experiments, simulations are conducted with predefined levels of these parameters to generate a dataset used for training regression models. Two types of regression models, linear and Gaussian process, are considered and compared. The study reveals that Gaussian process regression provides more accurate predictions for the selected output variables. Subsequently, the Gaussian process regression model is used for optimizing the design parameters. The optimization process incorporates cost functions defined for particular application, such as efficiency optimization for Passenger variant and performance optimization for Performance variant.

Keywords: permanent magnet synchronous machine, parameter study, Gaussian process regression, linear regression, sensitivity analysis, design optimization.

Acknowledgements

This study has been carried out with Associate Professor David Sedarsky as our examiner and Senior Lecturer Stefan Lundberg as our supervisor at Chalmers University of Technology, Sweden. We would like to thank our supervisors at Aurobay, Dhinesh V Velmurugan, Duc-Khanh Nguyen, and Alexandra Tokat for their constant support and technical insights on the topic, which helped us to learn and implement the knowledge that we've gained during this study. We would also like to thank Bertrend Kerres, Aurobay, for his insights on regression modelling.

Adithya Ram Panyam, Chanakya Panguluru, Gothenburg, 10 2023

List of Acronyms

Below is the list of acronyms that have been used throughout this thesis listed in alphabetical order:

AC	Alternating Current
BEV	Battery Electric Vehicle
CPSR	Constant Power Speed Region
DC	Direct Current
DoE	Design of Experiments
EDU	Electric Drive Unit
EV	Electric Vehicle
FEA	Finite Element Analysis
FEM	Finite Element Method
FDR	Final Drive Ratio
FWD	Front Wheel Drive
GPR	Gaussian Process Regression
IM	Induction Machine
IPMSM	Internal Permanent Magnet Synchronous Machine
LR	Linear Regression
MVLR	Multivariate Linear Regression
MTPA	Maximum Torque per Ampere
NMSE	Normalised Mean Squared Error
OA	Orthogonal Array
PMSM	Permanent Magnet Synchronous Machine
PM	Permanent Magnets
RMSE	Root Mean Square Error
RWD	Rear Wheel Drive
SE	Standar Error
WLTC	Worldwide Harmonised Light Vehicles Test Cycle

Nomenclature

Below is the nomenclature of indices, sets, parameters, and variables that have been used throughout this thesis.

Variables

m	Mass $[kg]$
m_{eff}	Apparent mass $[kg]$
v	Speed $[m/s]$
a	Acceleration $[m/s^2]$
g	Acceleration due to gravity $[m/s^2]$
A_f	Frontal Vehicle area $[m^2]$
ρ	Air density $[kg/m^3]$
c_r	Rolling resistance coefficient $[-]$
c_d	Drag coefficient $[-]$
α	Road gradient $[deg]$
F	Net force $[N]$
F_t	Tractive force at the wheels $[N]$
N_a	Synchronous speed of motor$[RPM]$
N_r	Rated speed of motor $[RPM]$
N_r	Speed of motor at peak power $[RPM]$
P	Number of poles per phase winding $[-]$
s	Slip of the motor $[-]$
ω_s	Electrical frequency $[Hz]$
p	Number of pole pairs $[-]$
(ψ_d, ψ_q)	d-axis and q-axis flux linkages $[Wb - turn]$
(I_d, I_q)	d-axis and q-axis component of phase current $[A]$
$V_{s,max}$	Maximum stator voltage $[V]$

$I_{s,max}$	Maximum stator current $[A]$
T	Torque $[N-m]$
T_r	Rated torque $[N-m]$
T_p	Peak torque $[N-m]$
T_{Ripple}	Torque ripple [%]
T_max	Maximum torque in torque fluctuation (ripple) $[N-m]$
T_max	Minimum torque in torque fluctuation (ripple) $[N-m]$
T_avg	Average torque $[N-m]$
h	Number of phases $[-]$
η_{WLTC}	WLTC cycle efficiency [%]
η_{system}	System efficiency [%]
η_{Rated}	System efficiency at rated operating point[%]

Parameters

Lm	Width of the bar magnet $[mm]$
Hm	Thickness of the bar magnet $[mm]$
Wb	Bridge thickness $[mm]$
Tj	Web length $[mm]$
θ	Angle between the V-shape magnets $[deg]$
Tw	Tooth width $[mm]$
FDR	Final drive ratio (gear ratio) $[-]$

Contents

List of Figures

List of Tables

1
Overview of Research Area

This chapter provides a brief overview of the research area which includes background, a summary of literature survey conducted in this study and the research objectives of this study.

1.1 Background

Battery electric vehicles (BEVs) are a promising alternative to traditional gasoline powered vehicles; BEVs utilize electrical energy stored in rechargeable batteries to power the drivetrain. The growing demand for electric vehicles is driven by reforms, laws and regulations aimed at reducing carbon emissions, and reliance on fossil fuels. BEVs offer numerous advantages, including lower carbon emissions, lower operating costs, and fewer maintenance requirements.

Despite their many advantages, electric cars have not been widely adopted yet due to their limited range, higher investment (upfront cost), and lack of infrastructure (charging stations) when compared to gasoline-powered vehicles. However, these drawbacks are being addressed with technological advancement in battery technology, manufacturing, and infrastructure development. Overall, electric cars represent a promising and rapidly developing technology that could play a crucial role in reducing carbon emissions and mitigating the effects of climate change in the years to come.

BEVs are propelled by electric motors; the most commonly used electric motors for vehicle application are Permanent Magnet Synchronous Machines (PMSMs) and Induction Machines (IMs) due to their high efficiencies and performance capabilities. While IMs offer high reliability and low cost, they have some limitations in the high speed range [1]. PMSMs are more capable when compared to IMs and have been adopted by many vehicle manufacturers. With this consideration, this study is focused towards optimizing the PMSM, recognizing its substantial impact on vehicle performance.

1.2 Literature survey

Significant amount of research has been conducted to improve the overall performance of PMSM by optimizing the geometric design parameters. In [1], Chen performed an individual and combined sensitivity analysis of six geometric parameters

of V shaped IPMSM (Internal PMSM) and concluded that the performance characteristics are very sensitive to some parameters and insensitive to others; it was found that width of the magnet and bridge thickness has the highest impact. In [2], Kim considered the ratio of pole-arc to pole-pitch and saliency due to duct structures to optimize the torque characteristics of a tangential-type IPMSM in their study. In [3], Kano studied the reduction in torque ripple when PM shape is changed from tangential to V-shaped PM in IPMSM. The research findings suggest that V-shaped PM configuration in PMSM is advantageous for BEV application and the findings also indicate that optimizing geometrical design parameters of the rotor can enhance the performance characteristics of PMSM. In [4], Xiaodong Sun performed a parameter study targeting stator geometry using FEA. The optimization of these parameters aimed at maximizing shaft torque while minimizing cogging torque and magnet volume. The optimized design of the PMSM was then fabricated and an experimental platform was developed to verify the test results which validated the optimization approach. In [5], Ahmadi presented a multi-objective optimal rotor design for a IPMSM where the primary focus was laid on torque optimization by testing the influence of several key factors such as permanent magnet arrangement, position and size. The optimal design was found by utilizing a cost function which aimed at maximizing average torque and minimizing torque ripple. The optimized design resulted in the increase of torque while the torque ripple reduced by 64%. In order to perform the parameter and sensitivity study a suitable baseline model of the PMSM which met the power requirements based on the use case of the vehicle is needed, in [6], Veiga provided insights on a strategy for sizing both an electric motor and battery pack for an automotive electric vehicle. In [7], Chin presents the study and the design analysis of a PMSM for the traction application of an electric vehicle by optimizing CPSR (Constant Power Speed Region) and flux by optimizing stator and rotor design parameters.

1.3 Research objectives

The objective of this study was to conduct a study on Electric Drive Unit (EDU), with a specific focus on the electric motor of EDU and optimize its design parameters. The objectives included analysing the design parameters of the motor in relation to vehicle performance characteristics and identifying sensitive design parameters through parameter sensitivity analysis. The study aimed to propose a methodology for optimizing the identified design parameters to improve vehicle performance. An appropriate optimization technique was incorporated to determine optimal design parameters. The optimized design parameters were evaluated using FEA simulations in Motor-CAD. The study provided recommendations and insights, emphasizing the potential impact of optimizing the selected design parameters on overall vehicle performance.

2
Introduction

This chapter provides an overview of basic working principles, types of electric motors, and the components of electric motors.

2.1 Principle of operation

Electric motors are electro-mechanical devices that convert electrical energy into mechanical energy based on the principles of electromagnetism. The principle of operation of electric motors is based on the fundamental relationship between electromagnetic fields and currents, enabling the conversion of electrical energy into mechanical motion. The underlying physical phenomenon behind motor operation can be explained with the help of Maxwell's equations of electromagnetism, a unified mathematical formulation that describes the behaviour of electric and magnetic fields, and Lorentz force equation that describes the interaction of charges/currents with electromagnetic fields.

Electric motors consist of two main components: a stationary part called stator, and a rotating part called rotor. The construction of these components depends on the type of the motor in question. The fundamental operating principle of a motor can be simplified as the interaction between the magnetic fields of the stator and rotor. Either of these components produce a rotating magnetic field and the magnetic field (own or induced) of the other component interacts with this rotating magnetic to generate torque. The stator typically consists of coils of wire wound around an iron core. These coils are connected to an external power source and carry an electric current. The rotor is either a permanent magnet or an electromagnet.

2.2 Types of electric motors

There are various types of types of electric motors that can be implemented in electric propulsion systems for BEVs. Different motor topologies like induction motors, permanent magnet synchronous motors, switched reluctance motors, brushed DC motors, and brushless DC motors have been used for BEV application [8], but the most commonly used motor topologies for commercial BEVs are IMs and PMSMs [9].

2.2.1 Asynchronous machines

The asynchronous motor commonly known as induction motor relies on a phenomenon known as slip. This refers to the difference in rotating speed of the rotating magnetic field in the stator and the rotating speed of the rotor and in turn the shaft. The rotor magnetic field will constantly try to align itself with the rotating magnetic field of the stator but will never catch up to it. This slip is used to induce rotor current in the rotor AC winding. As a result, the induction motor cannot produce torque near synchronous speed as induction ceases to exist as there is no slip.

The speed of the AC motor is determined primarily by the frequency of the AC supply and the number of poles in the stator winding, according to the relation:

$$N_a = \frac{120 \cdot \omega_s}{P} * (1 - s) \tag{2.1}$$

The synchronous speed of the motor can be calculated by removing the slip term $(1 - s)$ from the above equation. The slip for an induction machine is typically between 2% to 5%.

2.2.2 Synchronous machines

Synchronous machines are a class of machines where the rotor normally rotates at the same speed as the rotating magnetic field in the stator. The working principle of a synchronous motor is based on the interaction between the magnetic fields of the stator and rotor. The stator windings, when connected to a three-phase alternating-current supply, produces a rotating magnetic field with a speed calculated using equation (2.1). The rotor can produce its own magnetic field in one of two ways; either a direct current in the field winding of the rotor which will produce a magnetic field rotating at rotor speed based on Faradays Law or a permanent magnet in the rotor which produces a magnetic field. As the stator field rotates the rotor tries to align itself to the magnetic field while rotating the shaft. When the rotor speed is equal to that of the rotating stator magnetic field and there is no load torque, these two magnetic fields will tend to align with each other. When a mechanical load is applied, the magnetic field of the rotor lags behind by a few degrees with respect to the rotating field of the stator, this leads to a generation of torque and continues to try to align itself with the rotating field of the stator. The angle between the fields is directly proportional to the load torque. The maximum torque is produced when the angle by which the rotor field lags the stator field is 90°. If the load torque exceeds the maximum torque limit, it will lead to the stalling of the motor.

2.3 Permanent magnet synchronous machine

Permanent magnet synchronous machine, also known as PMSM is a type of synchronous motor where the rotation of the shaft is synchronized with the frequency of the supply current. It depends on the rotating magnetic field that generates electromotive force at synchronous speed. When the stator winding is energized by giving

the 3-phase supply, a rotating magnetic field is created in between the air gaps. This interacts with the magnetic field of the permanent magnets used in the rotor. As the stator of the motor which create a magnetic field that rotates in time with the oscillations of the current, the rotor with permanent magnets turns in step with the stator field at the same rate and as a result this produces the torque when the rotor field poles hold the rotating magnetic field at synchronous speed and the rotor rotates continuously. As these motors are not self-starting motors, it is necessary to provide a variable frequency power supply.

2.3.1 Parts of PMSM

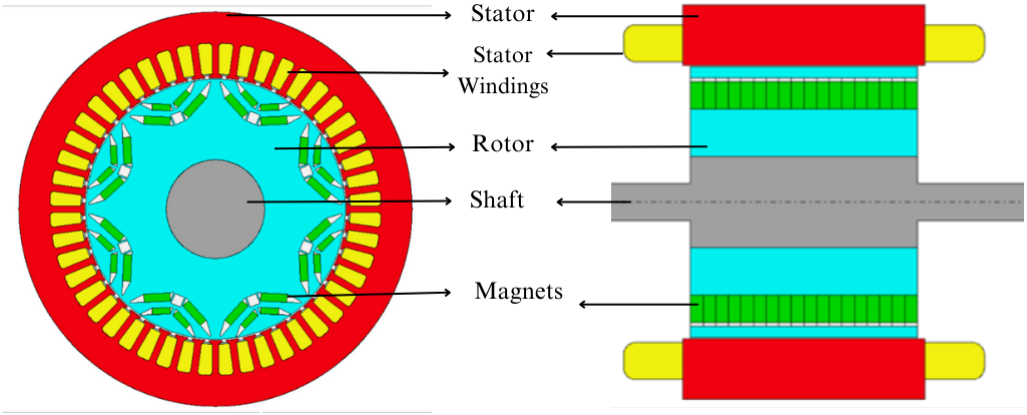

Figure 2.1: Parts of a PMSM

Stator: A stationary part in the electric motor which houses the entirety of the machine, including the rotor and windings. The windings are of a 3-Phase type that produces a sinusoidal electromagnetic field, which drives the rotor in a circular direction. The stator is designed using Motor-CAD, and consists of slots for the windings, the front and rear housing caps.

Rotor: The moving component in an electric machine which converts the electromagnetic force into circular motion. The by-product of this energy conversion is torque and is usually made of the same material as the stator, but in cases where weight is a factor, it is made of Aluminium. The rotor consists of a shaft connected to an external gearbox, V-web slots to aid in better magnetizing and magnets that assist in the torque delivery of the motor.

Stator winding: The winding on the stator delivers the EMF to drive the rotor with torque, which is also the component in an electric machine that generates heat due to current flow. The windings are done in a concentric method for the 3 phases, including the slots into which they overlap each other, creating multiple loops of windings which increase the magnetic force generation to produce torque at the stator. They winding is further designed by considering multiple parameters such as throw, turns and phases.

Magnets: The magnets are responsible for the magnetization of the electric machine. They are placed in the rotor lamination and can be configured in any way desirable. The magnetic field produced by the magnets is crucial for the operation of the machine.

Airgap: The air gap in a PMSM is the physical distance, generally 0.5-2mm between the rotor's permanent magnets and the stator windings, and it has multiple functions, it acts as a tolerance to enable the rotor to rotate without any friction, it allows for the interaction of the magenetic fields of the stator and rotor which leads to torque generation therefore having a significant impact on the motor's performance, efficiency, and overall operation.

Shaft: This is a solid metallic shaft which is connected to the rotor. As the rotor rotates, the shaft rotates along with it as is used to translate the rotational energy to the rest of the drivetrain.

3

Methodology

This chapter explains the methodology implemented in this study. The methodology consists of five steps. The first step was a pre-design step where the powertrain requirements were analysed based on the desired performance targets of the vehicle. The second step was to design a baseline PMSM motor in Motor-CAD and run simulations to conduct a parameter study and collect data required for building regression models. The parameter study includes a parameter sweep to identify the PMSM design parameters that were chosen for optimization. The third step was to build regression models of motor performance outputs with respect to the parameters identified in the previous step. Outputs like peak torque, peak power, rated efficiency, WLTC efficiency, torque ripple, and acceleration time (0-100 kmph) etc were chosen to build regression models. The acceleration time data was collected through the vehicle simulations run on GT-Suite. Using this regression models, the outputs for different combinations of design parameters were predicted and were used for optimization. The final step was to simulate a motor with the optimized design parameters and compare it with the baseline motor; a vehicle level simulation was performed in GT-Suite to analyse the performance improvement achieved by this optimization methodology. The overview of methodology is detailed in Figure 3.1.

3.1 Pre-design

First a short market survey of existing passenger and performance vehicles was conducted to understand the typical performance specifications and vehicle parameters of the vehicles in their respective segments. Vehicle parameters like frontal area, drag coefficient, tyre radius and final drive ratio for the desired vehicle were derived from this market survey. Then the desired vehicles 'Passenger variant' and 'Performance variant' were defined with a set desired performance specifications for the chosen vehicles parameters, Table 3.1.

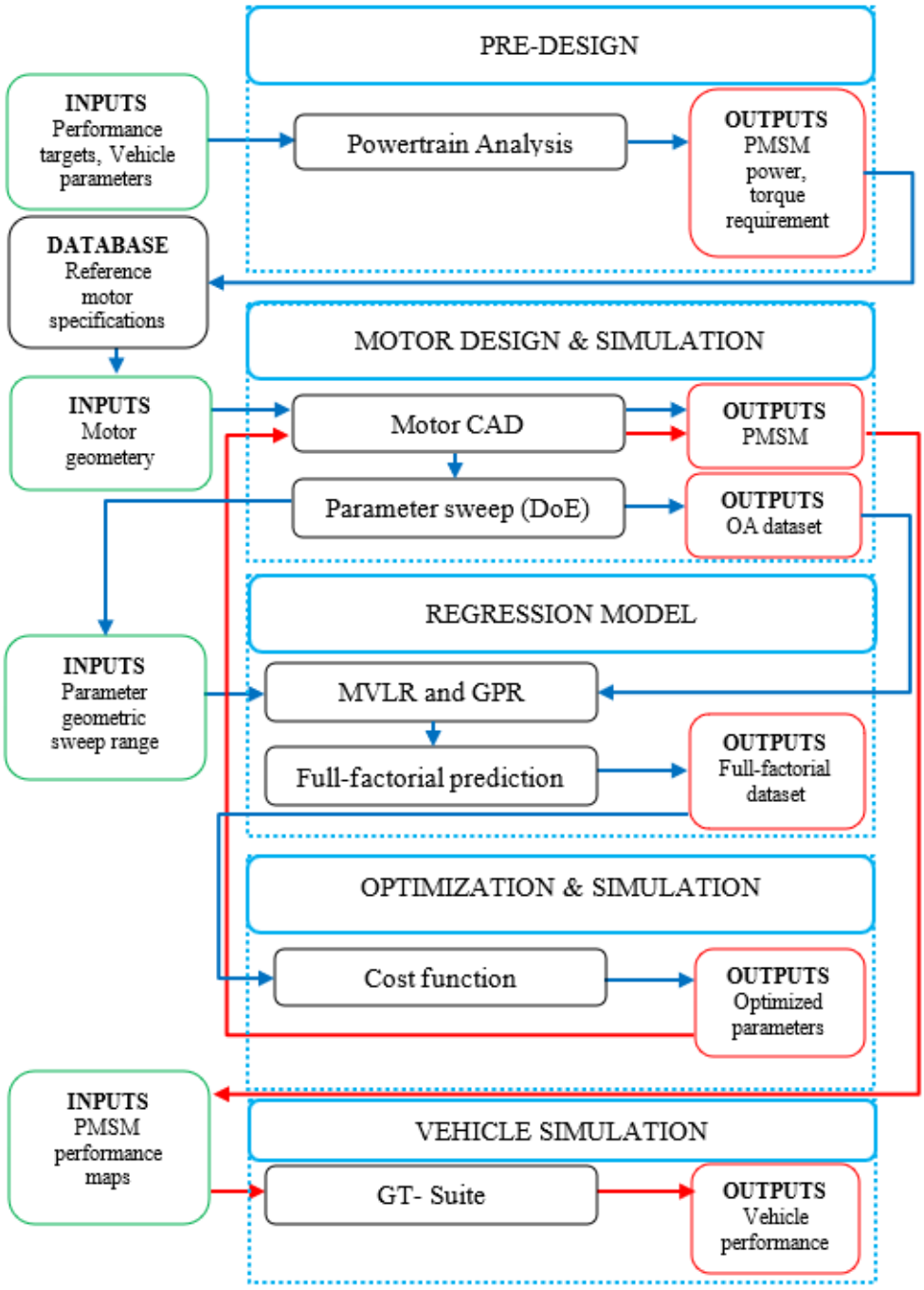

Figure 3.1: Overview of methodology used in this study.

Table 3.1: Vehicle parameters and powertrain requirements

Parameter	Unit	Passenger	Performance
Frontal area	m^2	2.40	2.33
Drag Coefficient	-	0.30	0.22
Tyre radius	mm	350	365
Peak shaft power	kW	140	240
Peak shaft torque	N-m	280	520
Gear ratio	-	9.74	8.05
Curb weight	kg	1800	2125
Maximum trailer weight	kg	1250	750
Top speed	km/h	180	230
Acceleration time	s	7.5	5.4

For Passenger variant the powertrain requirements chosen were top speed, uphill (with trailer) and acceleration, while for Performance variant only top speed and acceleration were considered. Using the equations of 1-D longitudinal vehicle dynamics, detailed in Section 4.1, the required power and tractive force at the wheels is calculated for both variants. Based on this requirements, power, torque, and speed requirements for PMSM were calculated using a fixed final drive ratio, Table 3.1.

3.2 Motor design & simulation

A reference motor was selected accordingly and was designed in Motor-CAD for further analysis and optimization. All geometric parameters of the motor were referenced from the design specification sheet provided by Aurobay. The parameters that were not provided in the specification sheet were assumed to ensure that the motor meets the target requirements. It must be noted that the data from specification sheet was only used as a reference and that the actual design implemented differs from the one contained in the specification sheet. The design considerations and methods chosen for motor modelling are provided in detail in Section 4.2.2.

Once the reference (baseline) motor was designed in Motor-CAD, a parameter study was conducted and the sensitivity of these parameters with respect to chosen outputs was studied. The parameter selection for this study was motivated from the literature survey summarized in Section 1.2. The parameter study was also used to identify the design range of variation for each parameter which was later required in design of experiments, Section 4.4.

3.3 Regression model

In this study, data based approach to optimization was chosen; statistical models built using regression techniques were incorporated. Two different regression models were considered: a linear regression model and a Gaussian process regression model.

Both models were compared for the same training and validation datasets and the model with higher predication accuracy was selected for optimization.

The training dataset for the regression models was generated by a set of simulations designed based on orthogonal array in Section 4.4. Whereas the validation dataset was generated with a random-walk approach where random combinations of design parameters were selected and simulated. The results of the validation set from both regression models were compared by calculating normalized mean squared error (NMSE) of the predicted outputs.

3.4 Optimization & simulation

The regression model selected for optimization was used to predict outputs like power, torque, torque ripple, efficiency, and acceleration time for a full factorial combination of the selected parameters. The predicted data was then used to choose the most optimal parameter combination by utilizing the defined cost function which was modelled based on the optimization objective for the respective variants. Explained in detail in Section 4.7.1. The prediction models were then evaluated by simulating the optimized parameter combination in Motor-CAD and by calculating the error in prediction and simulation.

3.5 Vehicle simulation

The performance maps of the optimized motor for both variants were extracted from Motor-CAD simulations and were used as inputs to the vehicle model built in GT-Suite. The desired vehicle performance targets that were defined in the pre-design step were then tested in GT-Suite simulation.

4

Modelling & Simulation

In this chapter, we present a comprehensive overview of modelling and simulation methods incorporated throughout our study. This includes the modelling and simulation methods essential for requirement analysis, motor design, regression models, and vehicle model.

4.1 Simulink powertrain model

Using 1-D longitudinal equations of motion, a simple vehicle model was built in Simulink. The forces considered to be acting on the vehicle were tractive force, aerodynamic force, rolling resistance and gradient force. The net force experienced by the vehicle is then given by the following equation.

$$F = F_t - \frac{1}{2}\rho A_f c_d v^2 - (mg\cos\alpha)c_r - (mg\sin\alpha) \tag{4.1}$$

The net force experienced by the vehicle is used to accelerate the vehicle, the equation above can be rearranged to calculate the traction force required at the wheels to accelerate the vehicle with an acceleration.

$$F_t = ma + \frac{1}{2}\rho A_f c_d v^2 + (mg\cos\alpha)c_r + (mg\sin\alpha) \tag{4.2}$$

Here, to account for apparent increase in mass due to inertial effect of rotating components of the powertrain, the mass of the vehicle is increased by 1%.

$$m_{\text{eff}} = 1.01 \times m \tag{4.3}$$

4.1.1 Top speed

The minimum continuous power required for the vehicle to travel at top speed on a flat road with zero acceleration was calculated using equation 4.2. The power and torque required from the motor for this scenario is just required to overcome aerodynamic force and rolling resistance. The torque and power for this requirement is usually low and is not a limitation while designing a motor since most electric motors can reach high speeds and the torque and power required at these speeds to maintain the top speed is usually quite low.

4.1.2 Up-hill towing

For this performance requirement, the uphill towing capacity of the vehicle is tested. The maximum allowable trailer mass was considered for this. The requirement was defined such that the vehicle will be able to tow the trailer at a certain road gradient and vehicle speed. This definition was based on design practices and methods at Aurobay. An increase in drag coefficient due to the trailer unit was also considered while calculating the forces. For passenger cars with low acceleration targets the peak power demand is usually required for this scenario and the torque demand is higher in case acceleration test scenario. For performance cars both peak power and peak torque demands are set by acceleration test scenario.

4.1.3 Acceleration

In this study for 0-100 kmph acceleration performance, the motor was operated at peak torque curve ensuring maximum torque at the wheels while accelerating. The Simulink model was used to estimate the peak torque curve required to reach a specified acceleration time for the given vehicle parameters. For this an initial guess of peak torque and peak power is required to estimate the acceleration time. The initial guess for peak torque and peak power was based on a numerical analysis of data of existing vehicles and their claimed acceleration time. A polynomial fit on this data is shown in the Figure 4.1. The total power (or torque) per mass of the vehicle is plotted against the 0-100 kmph acceleration time claimed by the manufacturer. The scale and polynomial curve equation for Figure 4.1 have been redacted from this report.

With this initial guess, time to accelerate was calculated and compared with the desired acceleration time. If the time to accelerate was more that the desired acceleration time the torque was increased in steps of 5 $N - m$ keeping the power constant and time to accelerate was calculated again and compared with desired acceleration time. This process is repeated until the time to accelerate was equal to (or just less than) our desired acceleration time.

The maximum power and torque requirement from the above three performance requirements is set as the minimum requirement from PMSM. The results from market survey (for vehicle parameters) and powertrain analysis are listed in Table 3.1.

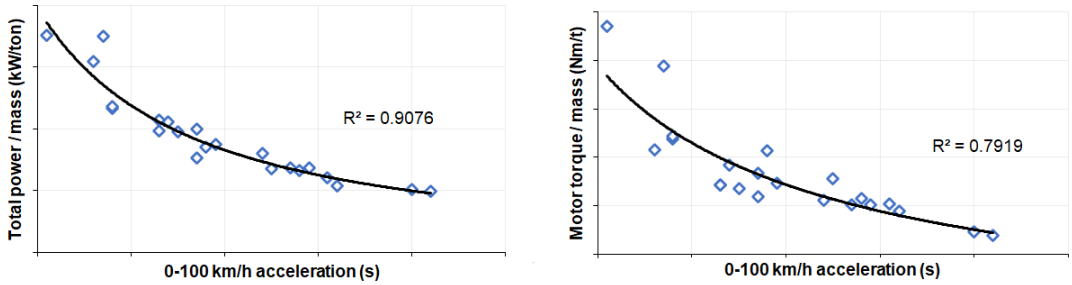

Figure 4.1: Power vs acceleration time and torque vs acceleration time for existing BEVs

4.2 Motor-CAD

MotorCAD is a comprehensive tool which is specifically utilized to design, assess and optimize the performance of an electric motor. It employs a multidimensional approach, integrating computational fluid dynamics and finite element analysis (FEA). This tool also possesses many features such as a Parameter Sweep tool, simulating the designed motor for any given drive cycle and allows for API scripting which aid us in our research. We utilized 2 types of models for our analysis. They are explained below:

1. **Electromagnetic Model** – This step of modelling includes the geometric design of the motor which includes the overall size and volume of the motor, the design of magnets and their placement and material used, widning etc. Following this, the software performs an FEM analysis by meshing the designed geometry and using analytical algorithms to simulate the working of the motor and the magnetic lines of force and their interaction to calculate the overall electromagnetic performance and output parameters at a particular operating point.
2. **Lab model** - The lab model captures the essential geometric and electrical characteristics of the motor and builds a model. This model helps in running vehicle level simulations of the designed motor and to generate crucial results such as efficiency maps, Torque-speed curves, drive cycle performance etc.

4.2.1 Motor-CAD calculation

The software simulates the electromagnetic behaviour of the motor using the finite element method (FEM) and computes several motor characteristics, including torque, efficiency, power, and flux linkage. The motor geometry, material used and operating conditions on which the motor must operate such as speed, voltage and current are defined. The software then computes the output characteristics of the motor by utilizing the governing equations of electromagnetism, such as Maxwell's equations and running FEM simulations to calculate the electromagnetic fields and forces present in the motor. Using a variety of analytical equations and algorithms. These outputs can be used to assess the motor's performance and enhance its design.

The major performance metrics which are being considered are calculated using the following formulas:

1. **Torque**: The electromagnetic torque is calculated based on *Maximum Torque per Ampere (MTPA)* control strategy, where for any operating point (given speed and current) in the Lab model, the maximum torque per ampere is determined. This aims to maximize torque for a given maximum current while considering the available voltage limit from the inverter. The formula is as follows:
$$T = \frac{h}{2} \cdot p \left(\psi_d I_q - \psi_q I_d \right) \tag{4.4}$$
Constraint:
$$\omega_s \sqrt{\psi_d^2 + \psi_q^2} \leq V_{s,\max} \quad \text{and} \quad \sqrt{I_d^2 + I_q^2} \leq I_{s,\max} \tag{4.5}$$
2. **Rated power**: This is the maximum power that the motor is designed to continuously deliver operate without damaging the motor due to temperature build up or other factors under normal operating conditions. This power limit is determined and limited by the motor's design, such as its size, cooling system, and material. The rated power of a PMSM is typically calculated using the following formula: The rated power (P_r) of a motor is given by:
$$P_r = N_r \cdot T_r \tag{4.6}$$
Where N_r is the rated speed in rad/sec and T_r is the rated torque (Nm).
3. **Peak power** (P_p) is the maximum power that the motor can deliver for a short period of time, without overheating or damaging the motor. Extended usage at this operating point can lead to damage. It is usually higher than the rated power and is often used to describe the motor's acceleration and torque capabilities. The peak power of a PMSM is typically calculated using the following formula:
$$P_p = N_p \cdot T_p \tag{4.7}$$
Where P_p is the peak power, N_p is the speed at which the peak power occurs, and T_p is the peak torque.
4. **System efficiency** is the ratio of the mechanical power at the output power by the motor at the shaft to the electrical power input to the motor, considering the losses in the motor and the inverter system. System efficiency (η_{system}) is calculated using the formula:
$$\eta_{\text{system}} = \left(\frac{P_{\text{out}}}{P_{\text{in}}} \right) \times 100 \tag{4.8}$$
5. **Torque ripple (T_{Ripple})** refers to the variation or fluctuation in torque output in a rotating system. For a PMSM, it's calculated as:
$$T_{\text{Ripple}} = \frac{T_{\max} - T_{\min}}{T_{\text{avg}}} \times 100 \tag{4.9}$$
Where T_{Ripple} is the torque ripple, $T_{\max}$ is the maximum torque, $T_{\min}$ is the minimum torque, and T_{avg} is the average torque.

4.2.2 Motor design

Based on the powertrain requirements derived in Section 4.1, and summarized in Table 3.1, a baseline motor model needs to be designed for Passenger variant and Performance variant. For this, a suitable reference model was selected from the available database of PMSM motor models, and the design parameters were adjusted to meet the requirements derived.

4.2.2.1 Passenger variant

For this study, an 8-pole interior V web double layer rotor was selected for the permanent magnet configuration. The double layer V-shape inter-web type rotor is a popular choice for PMSM's in passenger cars owing to its high-power density and efficiency. This rotor design is characterized by its unique V-shape arrangement of magnet poles that maximizes the flux linkage between the stator and rotor, resulting in high torque production and low cogging torque. Additionally, the double layer design further increases the torque density as there is an increase in the magnetic field lines and reduces the rotor's weight and size, making it an ideal choice as space and weight are critical factors.

Table 4.1: Motor Specifications

Type of Magnets	Interior V - Web
Poles	8
Magnet Layers	2
Air Gap	0.8

Table 4.2: Electrical Specifications

Voltage	550 V
Current	400 A
Phases	3
Type of Connection	Star

Table 4.3: Materials used in the PMSM

Stator Lamination	M250-3A
Armature Winding	Copper
Rotor Lamination	M250-3A
Magnet	N30EH

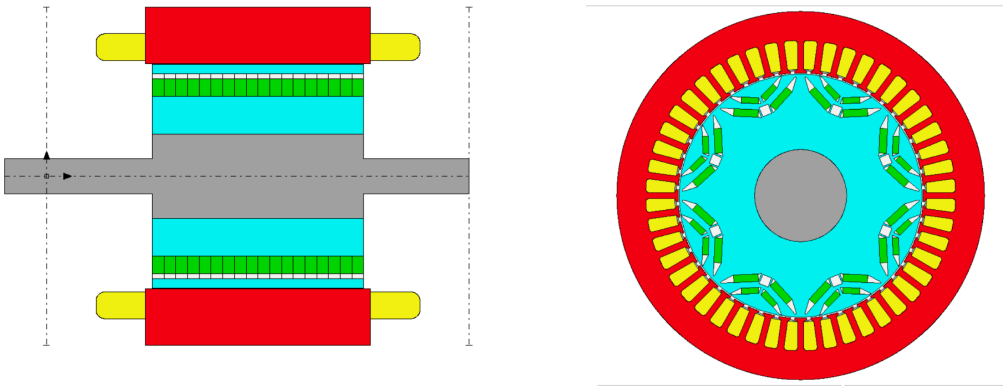

(a) Axial view **(b)** Radial view

Figure 4.2: Baseline motor - Passenger variant

The MTPA (maximum torque per ampere) control strategy, Section 4.2.1, was chosen for obtaining the motor performance characteristics. The torque-speed and power-speed characteristics of the motor are shown in Figure 4.3 and Figure 4.4 respectively. The peak torque achieved with this baseline design is 305 Nm and the peak power is 145.5 kW. We define the rated operating point as the point where field weakening occurs i.e. at the base speed of the motor (4274 RPM). At this operating point torque of the motor is same as the peak torque, and the power is is 135.8 kW. This torque and power will be referred to as rated torque and rated power in this report.

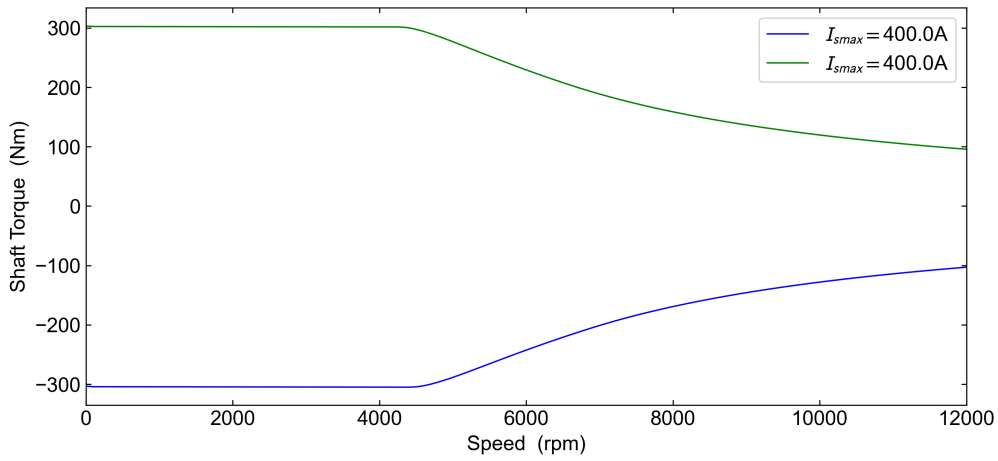

Figure 4.3: Torque vs speed of baseline motor for Passenger variant

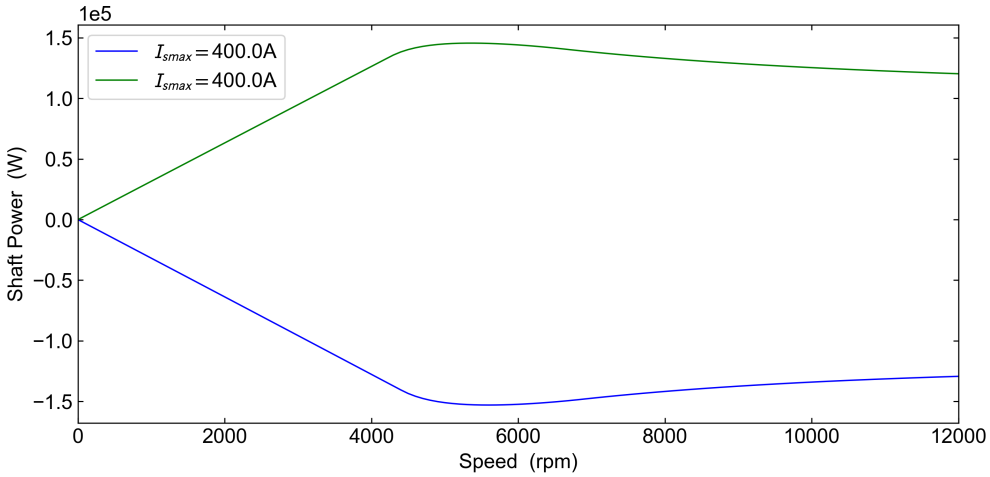

Figure 4.4: Power vs speed of baseline motor for Passenger variant

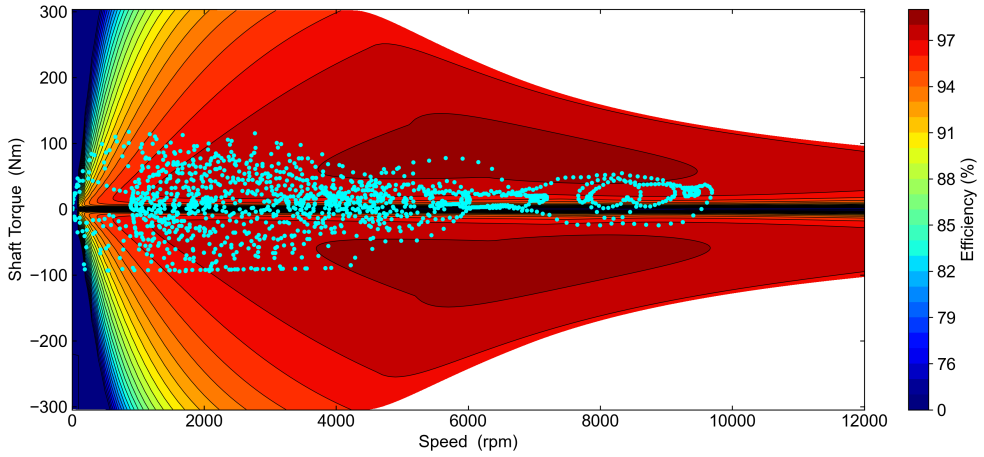

Figure 4.5: Efficiency map of baseline motor for Passenger variant

The efficiency map shows that the baseline motor is very efficient, and further analysis indicates that about 77% of the map area has an efficiency greater than 95%. The efficiency in low-medium torque range where most of the WLTC operating points lie, marked in cyan colour in the efficiency map, is also quite efficient ($\geq$ 95%). The point-to-point average efficiency of WLTC cycle is 94.66%. These metrics and the efficiency map will be later compared to that of the optimized motor in Section 5.1.

4.2.2.2 Performance variant

The PMSM used for the Passenger variant was appropriately scaled to fit the performance requirements for the Performance variant by increasing volume of the motor by increasing the diameter of the stator, the lengths and thicknesses of the 2 layers of the magnets were proportionally increased and the baseline variant was designed. Some of the properties and design characteristics are listed below. The designed

motor, when simulated reaches a peak torque of 534 Nm and a peak speed of 14000 rpm. The field weakening region starts at 4800 rpm.

Table 4.4: Motor Specifications

Type of Magnets	Interior V - Web
Poles	8
Magnet Layers	2
Air Gap	0.8

Table 4.5: Motor Specifications

Voltage	800 V
Current	450 A
Phases	3
Type of Connection	Star

Table 4.6: Materials used in the PMSM

Stator Lamination	M250-3A
Armature Winding	Copper
Rotor Lamination	M250-3A
Magnet	N30EH

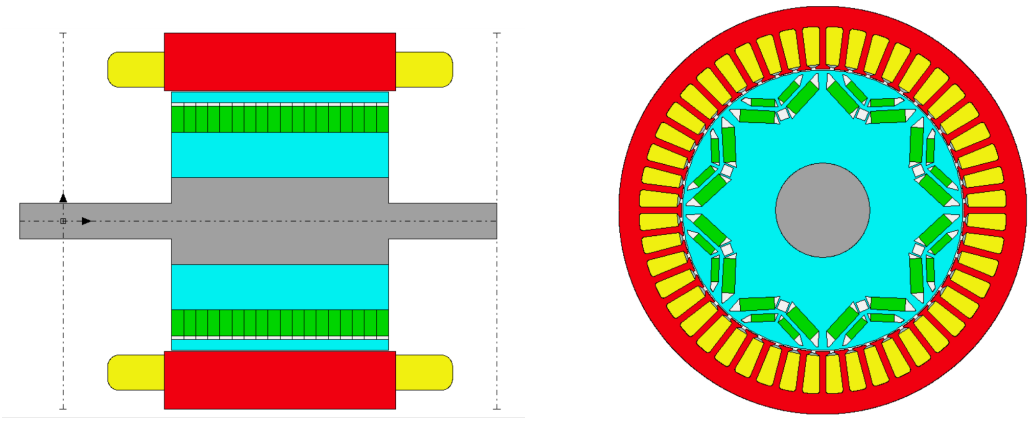

(a) Axial view **(b)** Radial view

Figure 4.6: Baseline motor - Performance variant

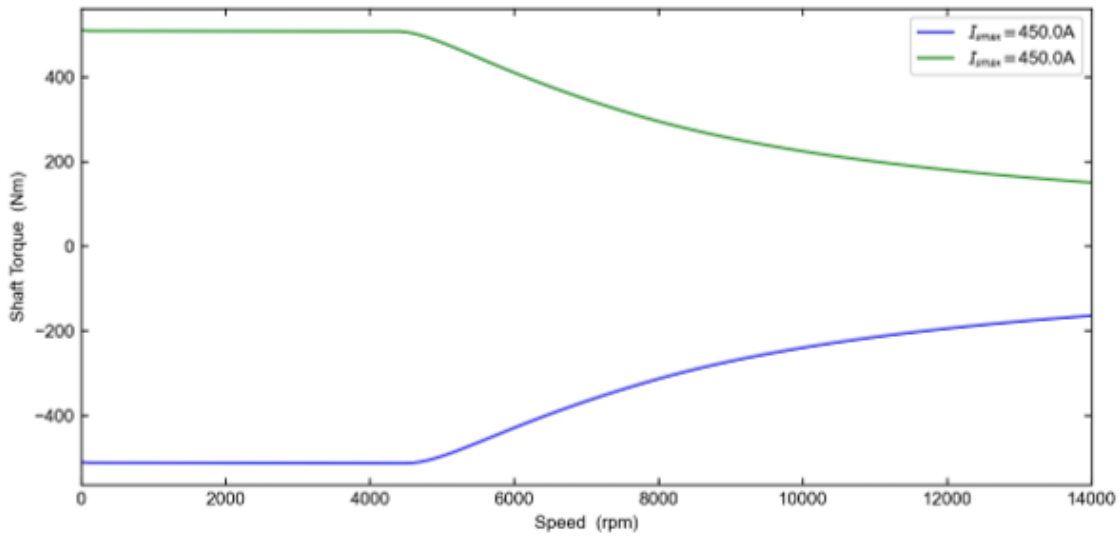

Figure 4.7: Torque vs speed of baseline motor for Performance variant

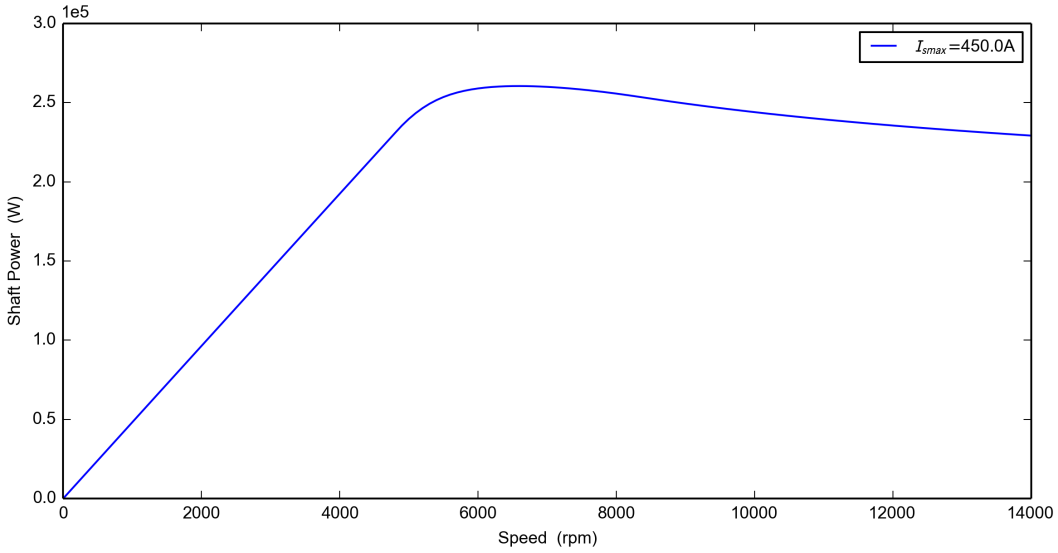

Figure 4.8: Power vs speed of baseline motor for Performance variant

The baseline motor for the performance follows a similar control strategy as the Passenger variant. As we can observe from fig and fig the peak shaft torque of the motor is slightly above 535 Nm and the peak power is 250 Kw which meets the demand for our application. The field weakening region begins at 4800 rpm which is referred to as base speed.

4.3 Parameter study

A parameter study is the systematic analysis of studying the effects on the output and the magnitude of its change of a model by varying its input parameters over a

range of values. The main objective of a parameter study is to explore how changing the values of certain parameters of a system affect the outputs of the model under investigation and to identify and study dependencies and to determine how sensitive the output is to the change in input parameters of the system. This information can be used to optimize the performance of the system or to gain a better understanding of its behaviour.

4.3.1 Parameter study of a PMSM

The parameter study of a PMSM for this study involves the investigation of the effects of varying the geometric parameter of the stator and the rotor on the performance characteristics of the PMSM. The vehicles have a power and torque requirement which needs to be met while reducing losses and increasing efficiency. In order to investigate which parameters have a significant effect on these key characteristics, a parameter study was performed.

For a PMSM, multiple parameters were included in the study after conducting a thorough literature survey, the focus of the parameter study was placed on geometric parameters with a focus on the dimensions and placement of the permanent magnets in the rotor. To perform the parameter study, the modelled PMSM is analyzed for different parameter combinations and the motor performance characteristics is simulated. This led to us observing some key behaviors of each parameter on the motor's characteristics, such as shaft torque, efficiency, and torque ripple. The following geometric parameters were chosen for the sensitivity study, shown in Figure 4.9. It should be noted that the final drive ratio (FDR) of the powertrain was also considered in this study to enable us to optimize the PMSM parameters more effectively while ensuring that the vehicle performance targets are met. Hence, the FDR can be treated as an additional parameter to the study which was later used in optimization process.

1. Lm – width of the magnet $[mm]$
2. Hm – thickness of the magnet $[mm]$
3. Wb – bridge thickness $[mm]$
4. Tj – web length $[mm]$
5. θ - angle between the V shape magnets $[deg]$
6. Tw - tooth width of the stator $[mm]$
7. FDR - final drive ratio $[-]$

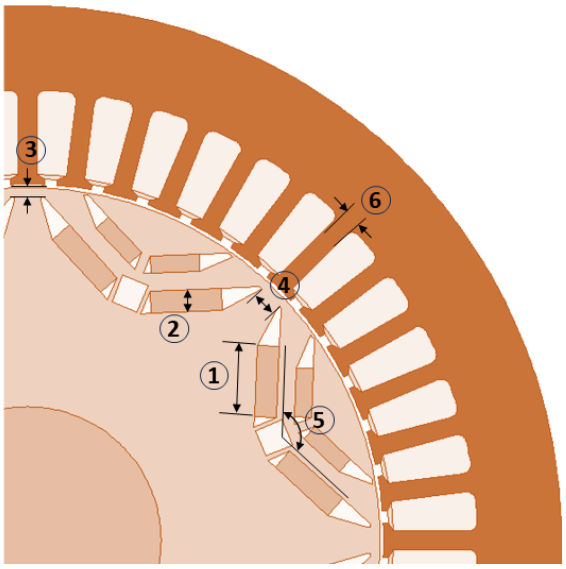

Figure 4.9: Parameters of the PMSM

4.3.2 Parameter sweep

A parameter sweep was conducted for the chosen parameters in Section 4.3 to understand how they affect the motors performance characteristics, studying the variation to choose an appropriate step size and the upper and lower geometric limits. This sweep was conducted by varying the parameters for a defined geometric range one at a time, while keeping the other parameters constant and their resulting torque, ripple and efficiency were plotted. The study was conducted by running at 3000 RPM at peak torque. The parameter variation and their effect on selected motor outputs are shown in Figures 4.10 - 4.12.

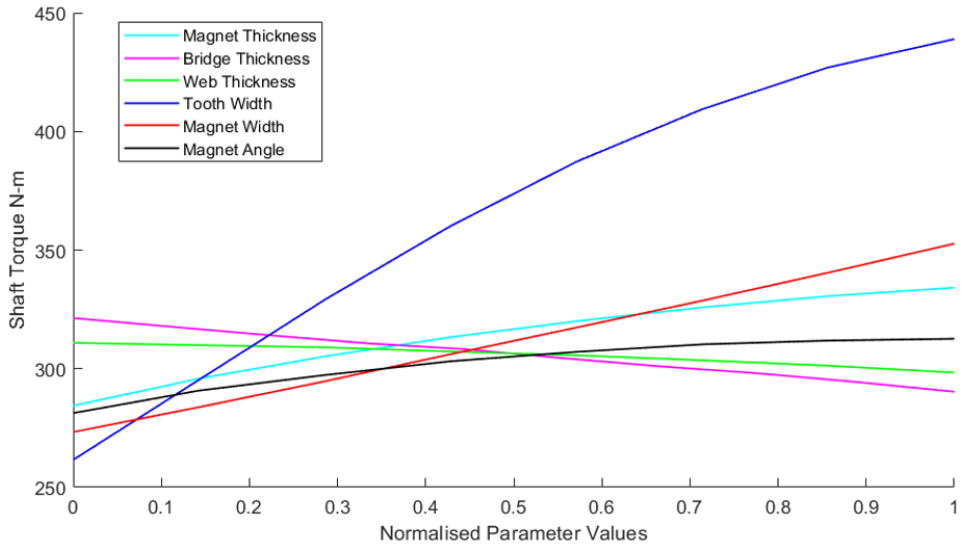

Figure 4.10: Variation of shaft torque with respect to the parameters

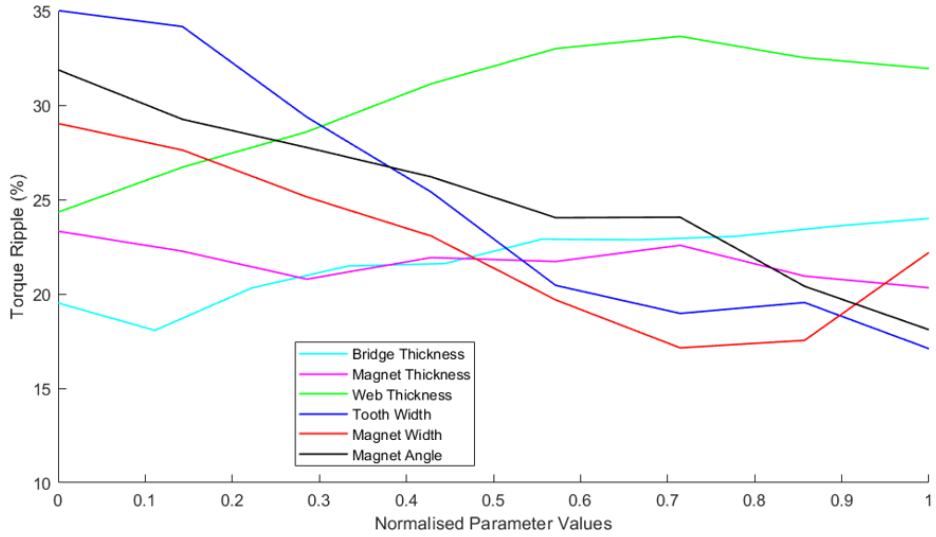

Figure 4.11: Variation of torque ripple with respect to the parameters

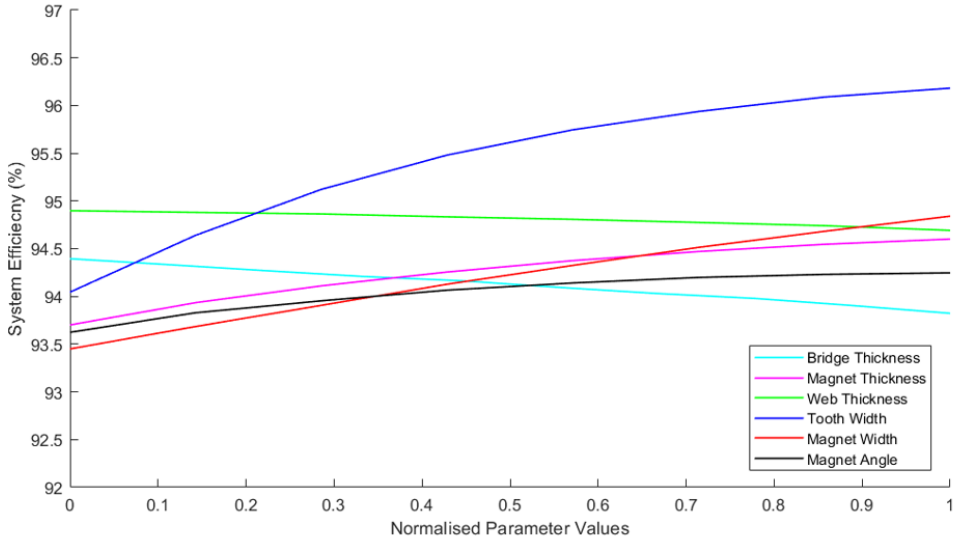

Figure 4.12: Variation of system efficiency with respect to the parameters

The parameter values were normalized linearly on a scale of 0 to 1, with respect to their minimum and maximum values (equation 4.10).

$$\hat{x} = \frac{1}{(x_{max} - x_{min})} \cdot x - \frac{x_{min}}{(x_{max} - x_{min})} \tag{4.10}$$

4.3.3 Observation from the parameter sweep

Observing Figure 4.10 and Figure 4.12 which depict the torque and efficiency variation with respect to changes in geometric parameters, it is clear that the relationship

between these parameters and torque and efficiency is fiarly linear in nature. When a parameter is increased or decreased within a certain range, the torque produced by the PMSM in the defined range, either increases, saturates or decreases accordingly, a similar trend is observed for efficiency. The Figure 4.11 which depicts the torque ripple variation with respect to changes in geometric parameters, it is evident that the relationship between these parameters and torque ripple is not always linear in nature. Instead, the torque ripple shows rise and falls as the geometric parameters are varied, indicating a complex and non-linear relationship. This suggests that optimizing the geometric parameters to minimize torque ripple in a PMSM may require more sophisticated modelling to account for the non-linear behavior and also highlights the importance of carefully considering the design parameters of the PMSM to ensure that the desired level of torque ripple is achieved.

By observing the behavior, a suitable step size and upper and lower limits of the geometric parameters needed to be chosen ensuring we do not ignore any variation in the behavior of the output. After a careful analysis where the non- linear behavior, geometric limits and tolerances were considered, the upper and lower limits of the geometric parameters were chosen, choosing a higher number of levels would increase the accuracy of the prediction but significantly increase the computational time. To strike a balance between these two factors 8 levels of variation were chosen between the limits.

4.4 Design of experiments

Design of experiments (DoE) is a systematic approach to investigate the individual and interactive effects of various input variables (also known as factors) on the outputs of a system or process under consideration. DoE allows researchers to efficiently identify and analyze key factors that influence the outputs while reducing the total number of experiments or simulations required. DoE can help ensure that experiments are appropriately controlled and are repeatable by offering a systematic approach to experimental design, which can enhance the validity and reliability of the results. In this study a DoE approach with orthogonal array (OA) was incorporated. The OA was designed based on Taguchi's OA construction as illustrated in [13], by Kacker.

In this study 7 design parameters were chosen and 8 levels were defined for each parameter. A full factorial parameter combination of these levels would result in a total of 8^7 (2,097,152) number of simulations which requires enormous computational time and resources. Hence, an OA appropriate for this study was designed which reduced the total number of simulations required to 64 simulations.

The OA used in this study is shown in Table 4.7. The complete OA is added in Appendix A.2. In OA, the coloumns represent differnet parameters and their respective levels for each simulation run (rows). For example, P_1 represents the pole angle, θ, of the PMSM and the value (0-7) assigned is the level of the parameter variation. The levels and their respective physical values are shown in Table 4.8.

The training dataset required for regression modelling is generated using this OA.

Table 4.7: Orthogonal array of experiments

Sim. no.	P_1	P_2	P_3	P_4	P_5	P_6	P_7
1	0	0	0	0	0	0	0
2	0	1	1	1	1	1	1
3	0	2	2	2	2	2	2
5	0	3	3	3	3	3	3
6	0	4	4	4	4	4	4
7	0	5	5	5	5	5	5
8	0	6	6	6	6	6	6
9	1	0	1	2	3	4	5
10	1	1	2	3	4	5	6
11	1	2	3	4	5	6	7
12	1	3	4	5	6	7	0
.	.	.	.	.	.	.	.
.	.	.	.	.	.	.	.
61	7	4	3	2	1	0	7
62	7	5	4	3	2	1	0
63	7	6	5	4	3	2	1
64	7	7	6	5	4	3	2

Table 4.8: Parameters and levels for Passenger variant

Parameter		**Unit**	**0**	**1**	**2**	**3**	**4**	**5**	**6**	**7**
P_1	θ	deg	95	101.5	107.9	114.3	120.7	127.1	133.6	140
P_2	Lm	mm	12	13.2	14.3	15.4	16.6	17.7	18.9	20
P_3	Hm	mm	4	4.5	5	5.5	6	6.5	7	7.5
P_4	Wb	mm	1	1.5	2	2.5	3	3.5	4	4.5
P_5	Tj	mm	2	2.6	3.3	3.9	4.6	5.2	5.9	6.5
P_6	Tw	mm	3	3.4	3.7	4.1	4.5	4.8	5.1	5.5
P_7	FDR	-	6.55	7.05	7.55	8.05	8.55	9.05	9.55	10.05

4.5 Multivariate regression

The objective of a regression problem is to learn input-output mappings from data (the training dataset). In this study the design parameters of PMSM selected in Section 4.3 are the inputs and motor performance characteristics like peak torque, peak power, torque ripple, efficiency etc., are the outputs that the regression model maps to the multiple variable inputs. In this study regression models were built for each of the motor outputs specified above.

The input variables are denoted as a vector $\mathbf{x}$ and the output is denoted by y. For a training set $\mathcal{D} = \{(\mathbf{x}_i, y_i) \mid i = 1, 2, \ldots, n\}$, where $\mathbf{x}_i \in \mathbb{R}^d$ and $y_i \in \mathbb{R}$,

the objective is to use the model to predict the outputs for a set of new inputs $\mathbf{x}^*$. In [10], Rasmussen explains how "we need to move from the finite data $\mathcal{D}$ to a function f that makes predictions for all possible input values" and that "we must make assumptions about the characteristics of the underlying function" to achieve this. In linear regression, the class of functions is restricted to linear functions of input. Whereas in Gaussian regression, probabilities are assigned to different possible functions (based on a prior probability) such that higher probabilities are assigned to functions that are more likely, "for example because they are smoother than other functions" [10].

In this section, both linear regression and Gaussian regression models are built using the training dataset and are compared to each other to check which model is best suited to model the outputs chosen for this study. This was achieved by comparing the normalized mean squared error (NMSE) of predicted outputs from the validation dataset. Once the regression model was selected, a full factorial prediction of outputs was generated and was used to optimize the input parameters according to the cost function defined in Section 4.7.1.

The predictor coefficients of the linear regression model were also used to investigate the sensitivity of the parameters with respect to specific outputs; and based on the optimization objective these parameters were ranked accordingly.

4.5.1 Linear Regression

Linear regression uses a linear predictor function whose model parameters, a set of coefficients, are estimated using the training dataset. As mentioned earlier, the class of function used is linear in nature, i.e., the predictor function is a linear combination of the coefficients and input variables [10]. The basic form of a linear predictor function f in matrix form is given by:

$$f(\mathbf{x}) = \mathbf{x}^T\boldsymbol{\beta} \tag{4.11}$$

where $\boldsymbol{\beta}$ is the coefficient vector $\boldsymbol{\beta} = [\beta_0\beta_1\beta_2 \dots \beta_m]$ and m denotes the number of variables in the input vector for any given observation i. The output for any given observation can be written as:

$$y_i = f(\mathbf{x}_i) + \varepsilon_i = \mathbf{x}_i^T\boldsymbol{\beta} + \varepsilon_i \tag{4.12}$$

where ε_i is an error variable that adds noise to the linear relationship between the dependent variable and predictor function. In this study, the MATLAB `fitlm` function was used to build the linear regression model, which uses the ordinary least squares approach to estimate the coefficient vector $\boldsymbol{\beta}$.

4.5.2 Gaussian Process Regression

Gaussian process is a probabilistic model approach towards regression [10] which is used to mathematically represent the relationship between input variables and outputs. Unlike linear regression model where a best-fit approach is used to build

the model and predict outputs for a set of new inputs, Gaussian process regression (GPR) uses Bayesian methods to provide a probability distribution of potential outputs rather than a single prediction.

GPR requires certain model parameters, like kernel functions and hyperparameters, as an input to the model. These model parameters determine the shape and features of the underlying functions within the Gaussian process. These kernels capture diverse relationships, like smoothness or periodicity. Hyperparameters of the kernel function are tuned through data-driven learning with the help of the training dataset. To predict outputs for a set of new inputs, GPR calculates the joint distribution of the training outputs and the new output. This joint distribution is a multivariate Gaussian distribution, where the mean represents the predicted value, and the variance indicates the uncertainty associated with the prediction. This approach to the regression technique works particularly well in small datasets while offering a comprehensive assessment of uncertainty in prediction.

In this study, MATLAB `fitrgp` function was used to build the GPR model. Through MATLAB's hyperparameter optimization, the `ardmatern32` kernel function was selected for this study. The mathematical form of the GPR model is given below [10].

For a training set $\mathcal{D} = \{(\mathbf{x}_i, y_i) \mid i = 1, 2, \ldots, n\}$, where $\mathbf{x}_i \in \mathbb{R}^d$ and $y_i \in \mathbb{R}$, a latent variable $f(\mathbf{x}_i)$ is introduced for each observation such that $\{f(\mathbf{x}), \mathbf{x} \in \mathbb{R}^d\}$ is a Gaussian process. Therefore, every finite linear combination of $\{f(\mathbf{x}), \mathbf{x} \in \mathbb{R}^d\}$ is normally distributed. An explicit basis function $\mathbf{h}$ is then used to transform the input variable vector $\mathbf{x}_i \in \mathbb{R}^d$ to vector $\mathbf{h}(\mathbf{x}_i) \in \mathbb{R}^m$. In vector form, a Gaussian process regression model can be represented as:

$$P(y_i|f(\mathbf{x}_i), \mathbf{x}_i) \sim \mathcal{N}(y_i|\mathbf{h}(\mathbf{x}_i)^T\boldsymbol{\beta} + f(\mathbf{x}_i), \sigma^2) \tag{4.13}$$

4.5.3 Comparison of regression models

The training dataset for regression models was generated through simulations performed on Motor-CAD and GT Suite (to simulate acceleration time), using the OA of experiments. To evaluate the accuracy of the regression models, a validation dataset consisting of 15 simulations was generated by using a random-walk approach. First, the MATLAB function `randi` was used to generate a random set of parameter combinations within the parameter ranges defined in Table 4.8. It was also ensured that the parameters can assume intermediate values between the levels defined in Table 4.8. This method was employed because it reduces bias and provides a more accurate estimate of model performance and is easy to implement. The validation set of parameter combinations was then simulated on Motor-CAD and GT Suite to generate validation dataset. The model predictions for the training and validation datasets, for the Passenger variant, are shown in Figures 4.13 - 4.18.

The predictions for peak shaft torque, peak shaft power, and acceleration time shown in Figures 4.13, 4.14, and 4.15 respectively are the most crucial for the optimization

method incorporated in this study. Since these predictions were used to filter out the parameter combinations that do not meet the vehicle performance targets. It can observed that Guassian process regression performs better than linear regression for these outputs on both training dataset and validation dataset, particularly so in the prediction of acceleration time.

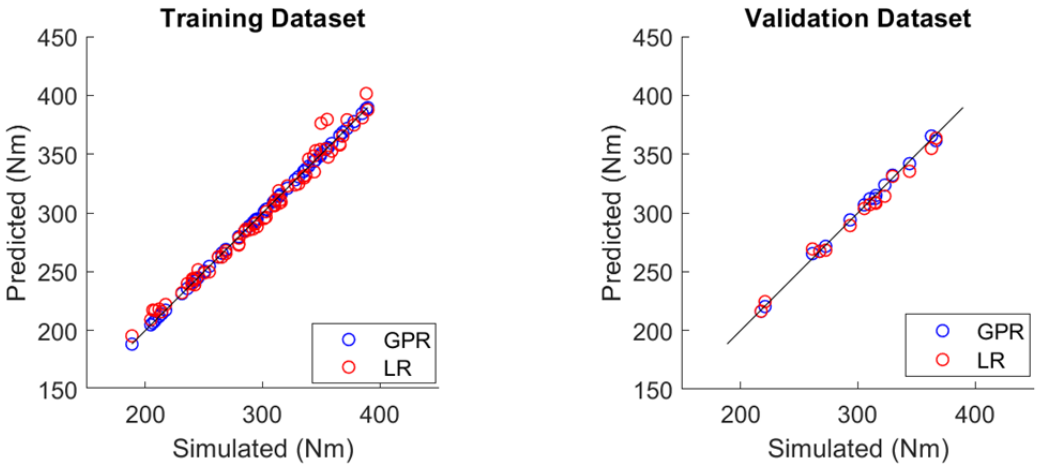

Figure 4.13: Peak shaft torque for Passenger variant

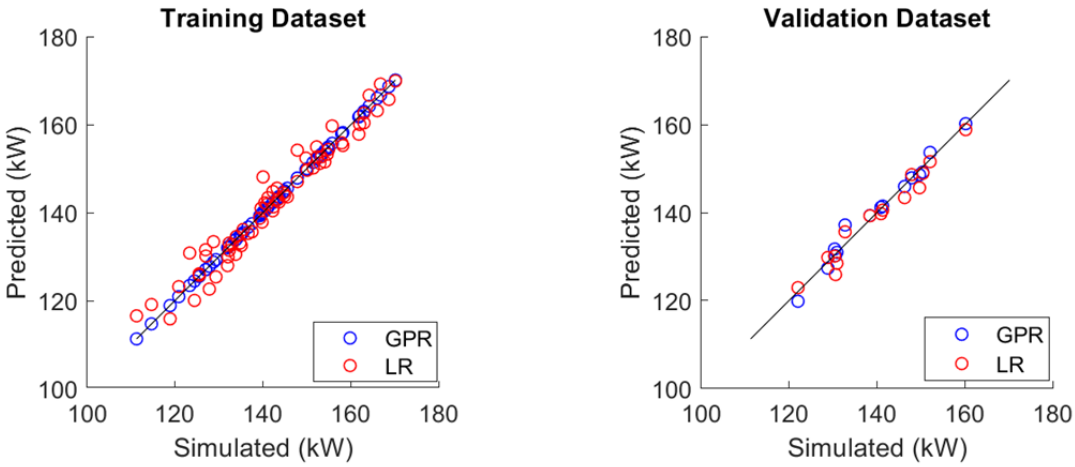

Figure 4.14: Peak shaft power for Passenger variant

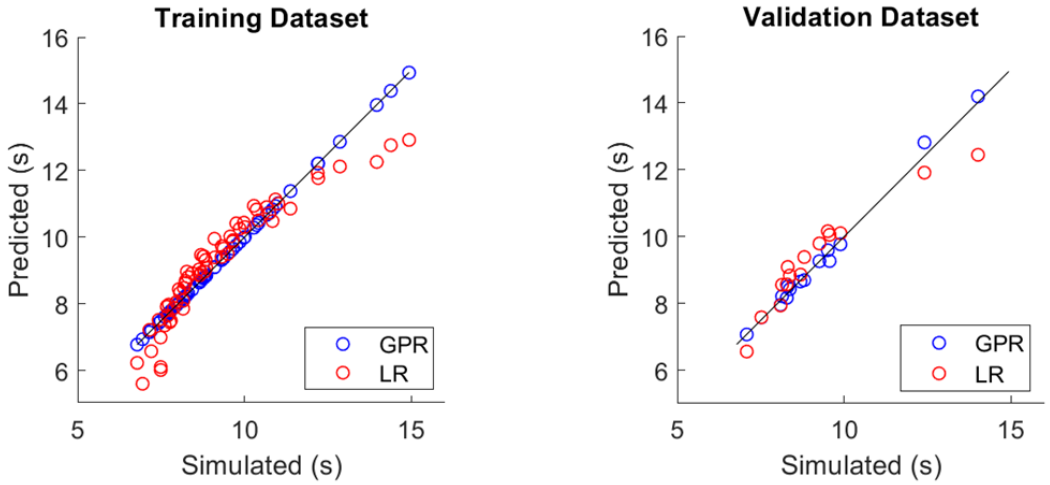

Figure 4.15: Acceleration time (0-100kmph) for Passenger variant

The predictions for torque ripple, rated efficiency, and WLTC cycle efficiency shown in Figures 4.16, 4.17, and 4.18 respectively were used for the optimization objectives and hence it is also crucial to ensure that these predictions were as accurate as possible. It can be observed that the Gaussian process regression performs considerably better on the training dataset and that both Gaussian process regression and linear regression have similar prediction accuracy on the validation dataset.

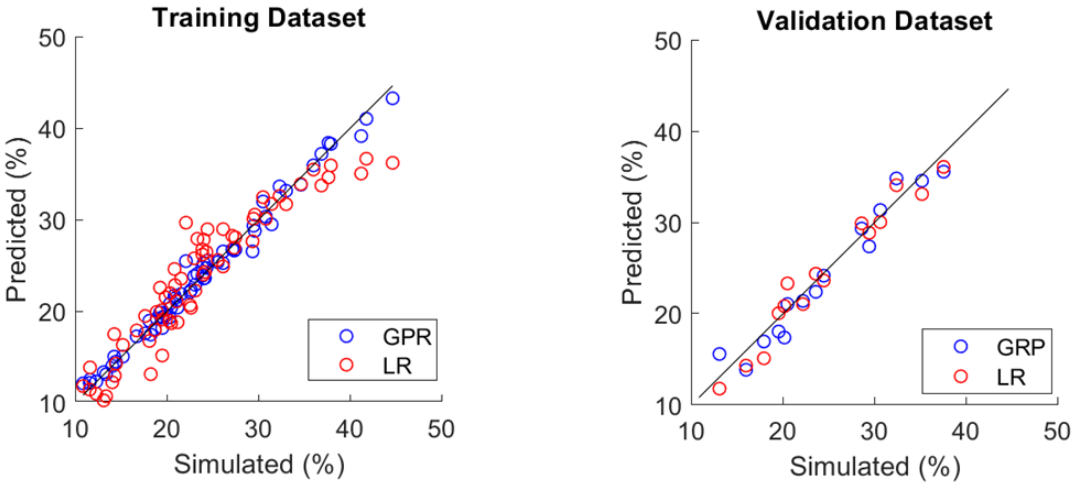

Figure 4.16: Torque ripple (at rated operating point) for Passenger variant

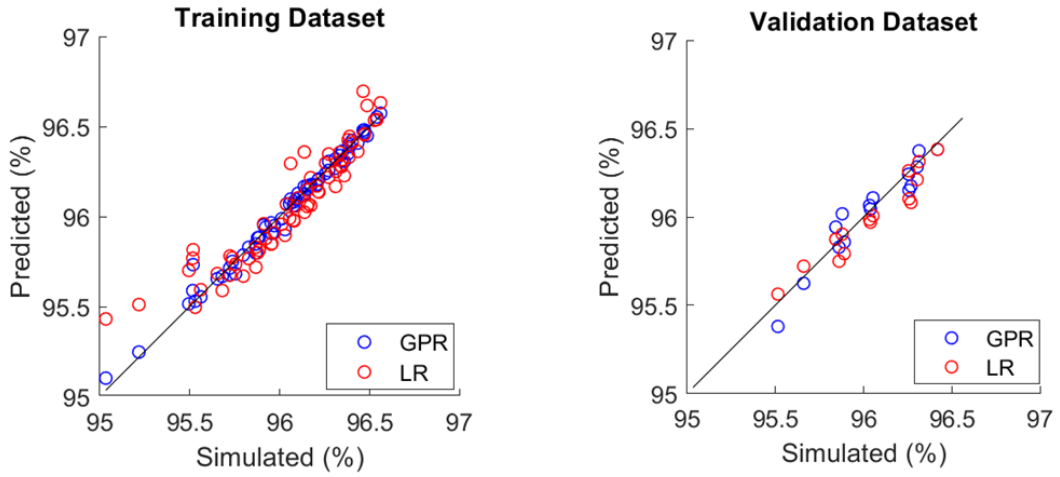

Figure 4.17: Rated efficiency for Passenger variant

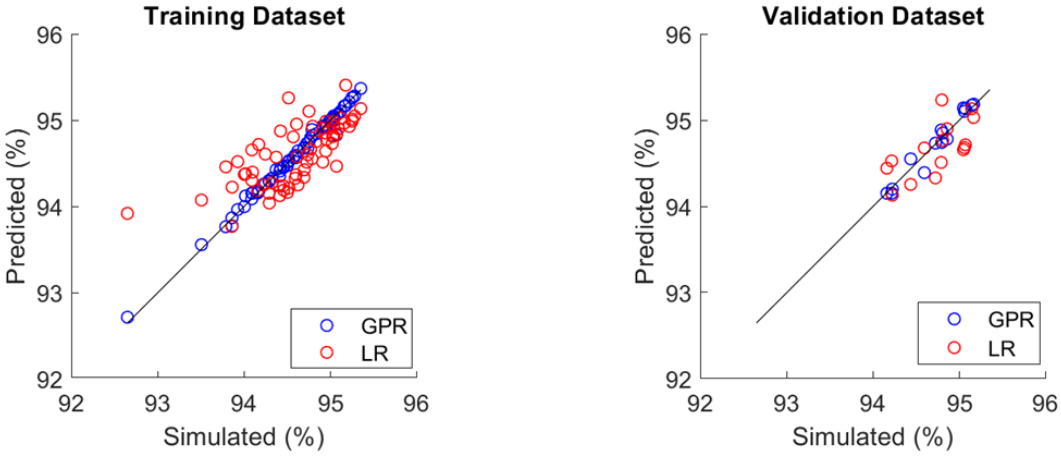

Figure 4.18: WLTC cycle efficiency for Passenger variant

To compare both regression models quantitatively, a weighted average of NMSE of all the outputs mentioned above was calculated with higher weight assigned to NMSE of shaft torque, peak shaft power, and acceleration time. The formula used for calculating NMSE is shown in Eq. 4.14, where both $\hat{y}_{pred,i}$ and $\hat{y}_{sim,i}$ are normalized values and N denotes the number of observations (or simulations). The NMSE for all the outputs are shown in Table 4.9.

$$\text{NMSE} = \frac{1}{N}\sum_{i=1}^{N}(\hat{y}_{\text{pred},i} - \hat{y}_{\text{sim},i})^2 \tag{4.14}$$

Table 4.9: NMSE on validation dataset

Output	Linear regression	Gaussian process regression
Peak torque	0.0009	0.0003
Peak power	0.0032	0.0026
Acceleration time	0.0335	0.0004
Torque ripple	0.0057	0.0065
Rated efficiency	0.0089	0.0109
WLTC cycle efficiency	0.0716	0.0055

Gaussian process regression has lower averaged NMSE and hence it was concluded that it is the best suited model for the optimization method incorporated in this study. However, the regression coefficients of the linear regression model was used to conduct a sensitivity study on the parameters chosen for this study. This method of sensitivity analysis was chosen since the first-order sensitivity can be easily derived by performing hypothesis tests on the coefficients of linear regression model. The equations obtained from linear regression modelling are attached in the Appendix A.2.

4.6 Sensitivity study

Sensitivity study or sensitivity analysis is a technique used to determine the significance of a particular input to the output of a model, which helps in gaining insights on how changes in particular input variable affects the output of a model. It helps to understand how sensitive the model is to changes in the inputs. Sensitivity analysis is mainly used to identify which input variables have the greatest impact on the output and provides information about which input variables can be altered without significantly affecting the output. This information can play a key role in re-designing the model for optimization.

A sensitivity analysis of the geometric parameters in a PMSM help us to identify the most critical geometric parameter that have the greatest impact on the performance of the motor of the selected 6 parameters. This will give us a general understanding of how the motor would behave for the change of the parameters and aid us in varying parameters to accurately size the motor. By identifying the critical parameters, it helps us to focus our efforts on optimizing these parameters to improve the performance of the motor.

In this case, the coefficient of the equations obtained from linear regression was used to perform first-order sensitivity study and rank the parameters according to their sensitivity and signifinace on outputs. *t-statistic* for each coefficient was used to test the null hypothesis that the corresponding coefficient is zero against the alternative that it is non-zero, calculated according to the simplified Equation 4.15 where *SE* denotes the standard error of the estimated coefficient. The two-sided *p-value* for the *t-statistic* was then used to derive the significance level. In this study, the significance level was set to 5%. The linear regression model built in Section 4.5.1

using the MATLAB function `fitlm` includes the values *SE*, *t-statistic*, and *p-value* for estimated coefficient for each of the parameters chosen for this study.

$$\text{tstat} = \frac{coefficient}{SE} \tag{4.15}$$

This method can be used directly for individual sensitivity analysis, i.e. to study sensitivity of parameters with respect to a specific output. However, to rank the parameters based on their sensitivity with respect to multiple outputs, the optimization objective function or cost function defined in Section 4.7.1 was used to study combined sensitivity.

4.6.1 Individual Sensitivity Study

In order to compare the sensitivity of these parameters with each other and to compare the sensitivity across different outputs, both parameter values and the output values were normalized (equation 4.10). The normalized coefficient values and their respective *t-statistic*, and *p-value* for each of the parameters are tabulated below, Table 4.10 - Table 4.17. The normalized coefficient value for each parameter is also represented in the bar graphs, Figure 4.19- Figure 4.22. In these figures, bar graphs coloured in red indicate that the *p-value* for the corresponding parameter is ≥ 0.05 and that the effect of the parameter on the output is statistically insignificant. The equations derived from linear regression modelling are added in Appendix A.2

`NOTE:` The first-order partial derivatives of the linear regression models, Appendix A.2, are the sensitivity coefficients. The sign of these coefficients was retained by not taking the absolute value, in an attempt to investigate the nature of the effect of each parameter on the outputs as shown in the bar graphs below. A positive coefficient indicates that for a positive change in parameter, the output also shows a positive change, and vice versa.

`NOTE:` The analysis and inferences made within this section is only applicable for the defined range of parameters, Table 4.8. However this method can be used to study the sensitivity of other parameters or other parameter ranges as desired.

The bar graph for torque, Figure 4.19 (a), shows that tooth width of the stator has the highest influence on torque and that the effect of pole angle is insignificant. Whereas the bar graph for peak power, Figure 4.19 (b), shows that the magnet width has the highest influence on peak power. It can be observed that variation in the parameters have similar effect on both torque and peak power, for example increasing the magnet width increases both torque and peak power.

Table 4.10: Regression coefficients and p-values for peak torque

Parameter	Coefficient	p-value
Pole angle	0.0156	0.26
Magnet width	0.2409	~ 0
Magnet thickness	0.0665	~ 0
Bridge thickness	-0.1719	~ 0
Web thickness	-0.0384	0.007
Tooth width	0.6948	~ 0
Gear ratio	-	-

Table 4.11: Regression coefficients and p-values for peak power

Parameter	Coefficient	p-value
Pole angle	0.1118	~ 0
Magnet width	0.5487	~ 0
Magnet thickness	0.1903	~ 0
Bridge thickness	-0.3711	~ 0
Web thickness	-0.1228	~ 0
Tooth width	0.06077	0.004
Gear ratio	-	-

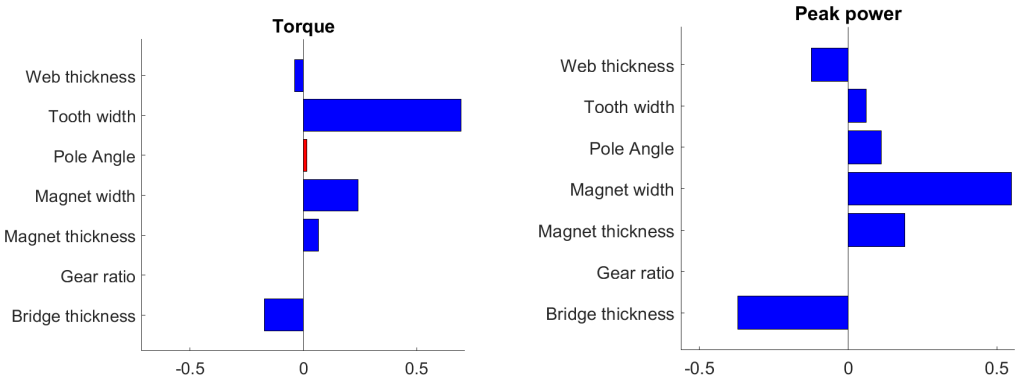

Figure 4.19: Regression coefficients for peak torque and peak power

As observed earlier tooth width has significant effect on torque and hence it effects acceleration time. The bar graph for acceleration time, Figure 4.20 (a), shows that the final drive ratio also has significant effect on 0-100 kmph acceleration time of the vehicle. In 4.20 (b), it is interesting to note that all parameters except tooth width have no effect (statistically insignificant) on the base speed of the PMSM. From these two figures it can be inferred that while the base speed decreases with increase in tooth width, the acceleration time will reduce by increasing tooth width and final drive ratio.

Table 4.12: Regression coefficients and p-values for acceleration time (0-100 kmph)

Parameter	Coefficient	p-value
Pole angle	-0.0612	0.052
Magnet width	-0.2163	∼0
Magnet thickness	-0.0789	0.017
Bridge thickness	0.1311	∼0
Web thickness	0.0394	0.21
Tooth width	-0.4124	∼0
Gear ratio	-0.3080	∼0

Table 4.13: Regression coefficients and p-values for base speed

Parameter	Coefficient	p-value
Pole angle	0.0177	0.45
Magnet width	0.0191	0.43
Magnet thickness	0.0216	0.36
Bridge thickness	-0.0088	0.71
Web thickness	-0.0281	0.23
Tooth width	-0.8971	∼0
Gear ratio	-	-

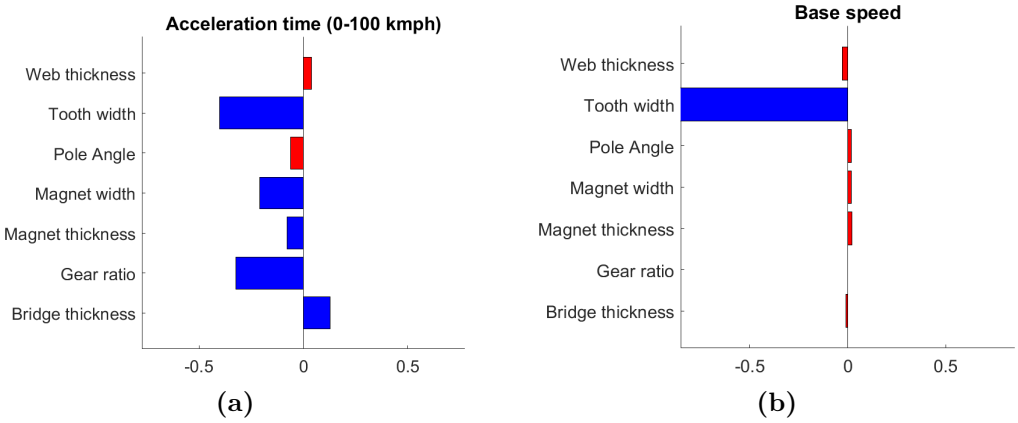

Figure 4.20: Regression coefficients for acceleration time and base speed

From Figure 4.21 (a), it can be observed that tooth width has highest influence on air gap flux density and that all other parameters have no considerable effect. The torque ripple graph, Figure 4.21 (b), suggests that torque ripple is more dependent on the distances that affect the interaction between magnets and stator than the volume of magnets used. Magnet width, magnet thickness and pole angle have no effect (statistically insignificant) on torque ripple.

Table 4.14: Regression coefficients and p-values for air-gap flux density (mean)

Parameter	Coefficient	p-value
Pole angle	-0.0175	0.37
Magnet width	0.0459	0.03
Magnet thickness	0.0061	0.76
Bridge thickness	-0.0623	0.002
Web thickness	0.0185	0.35
Tooth width	0.7999	∼0
Gear ratio	-	-

Table 4.15: Regression coefficients and p-values for torque ripple (at rated operating point)

Parameter	Coefficient	p-value
Pole angle	-0.0593	0.0695
Magnet width	0.0181	0.5886
Magnet thickness	-0.0225	0.4882
Bridge thickness	-0.2479	∼0
Web thickness	0.3381	∼0
Tooth width	-0.5063	∼0
Gear ratio	-	-

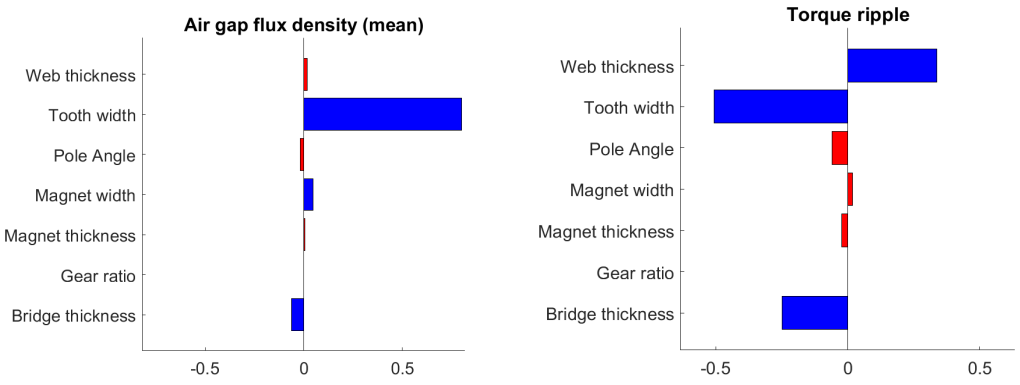

Figure 4.21: Regression coefficients for air-gap flux density (mean) and torque ripple (at rated operating point)

In Figure 4.22, the sensitivity of parameters with respect to rated efficiency and WLTC cycle efficiency is shown. Varying the final drive ratio shifts the operating points of WLTC cycle within the operating region of motor efficiency map, for example if the final drive ratio is increased the operating points marked in cyan colour in Figure 4.5 would shift closer to the *x-axis* and result in a lower WLTC cycle efficiency. This can be observed in the bar graph also, Figure 4.22 (b). However, it can be observed that this effect of final drive ratio on the WLTC cycle efficiency

is statistically insignificant for the range of final drive ratios defined in this study, Table 4.8. Another interesting observation that can be made is that higher volume of magnets result in higher rated efficiency whereas as the opposite can be observed for WLTC cycle efficiency.

Table 4.16: Regression coefficients and p-values for efficiency (at rated operating point)

Parameter	Coefficient	p-value
Pole angle	0.0554	0.079
Magnet width	0.4625	∼0
Magnet thickness	0.1531	∼0
Bridge thickness	-0.3028	∼0
Web thickness	-0.1006	0.002
Tooth width	0.1543	∼0
Gear ratio	-	-

Table 4.17: Regression coefficients and p-values for WLTC cycle efficiency

Parameter	Coefficient	p-value
Pole angle	-0.0622	0.23
Magnet width	-0.1747	0.002
Magnet thickness	-0.0199	0.71
Bridge thickness	0.1234	0.02
Web thickness	0.0377	0.47
Tooth width	0.3547	∼0
Gear ratio	-0.0957	0.08

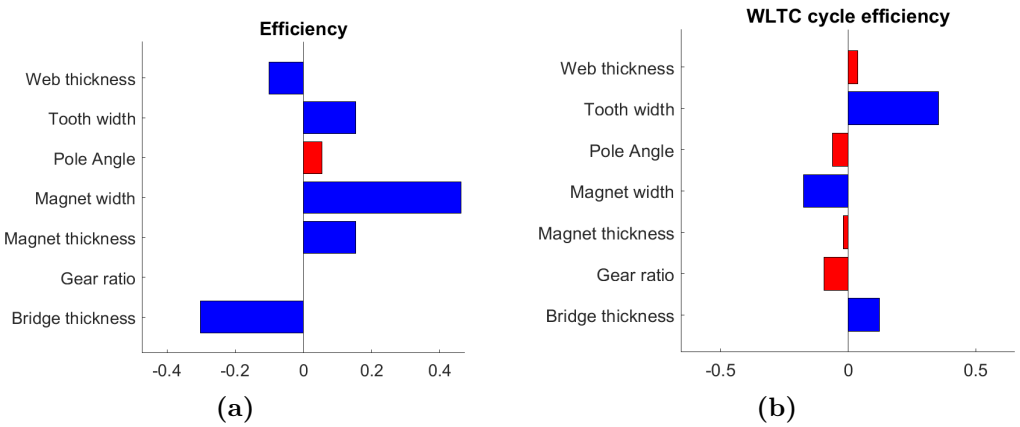

Figure 4.22: Regression coefficients for efficiency (at rated operating point) and WLTC cycle efficiency

This analysis helped in identifying the parameters that exerted significant effect and the ones that had a relatively minor effect on outputs. Among these parameters,

the tooth width and the magnet width emerged as the parameters having the most significant effect on performance outputs. In contrast, the pole angle, as reflected by its corresponding effects in the bar graphs, demonstrates a notably minor effect on performance, establishing it as a parameter of lesser significance.

4.6.2 Combined sensitivity

The combined sensitivity analysis of geometric parameters for a PMSM presented in this section provides a holistic perspective on the relationships between the parameters and performance characteristics of the powertrain. The individual sensitivity analysis gave us insights on how significantly parameters affected a single output of the motor. Utilizing these results, a comprehensive overview of the collective influence of multiple parameters on multiple outputs simultaneously was done by integrating the outcomes of these individual analyses and finding the 'average effect' that a parameter has on multiple outputs. A weighted average, by combining the coefficients of different outputs, listed in Table 4.18, was calculated to determine the 'average effect' a parameter has on these outputs. These outputs were selected according to the objective function (or cost function) defined, in Section 4.7.1, for specific vehicle application.

Table 4.18: Weights for calculating coefficient average for combined sensitivity

Passenger		**Performance**	
Output	**Weight**	**Output**	**Weight**
WLTC efficiency	0.4	Rated efficiency	0.4
Torque ripple	0.2	Torque ripple	0.4
Magnet weight	0.4	Magnet weight	0.2

Table 4.19: Weighted average of regression coefficients for Passenger Variant

Parameter	**Coefficient**
Pole angle	-0.0448
Magnet width	0.1159
Magnet thickness	0.2067
Bridge thickness	0
Web thickness	0.0848
Tooth width	-0.0393
Gear ratio	-0.0382

Table 4.20: Weighted average of regression coefficients for Performance variant

Parameter	Coefficient
Pole angle	-0.0056
Magnet width	0.2833
Magnet thickness	0.1618
Bridge thickness	-0.2201
Web thickness	0.0961
Tooth width	-0.1415
Gear ratio	0

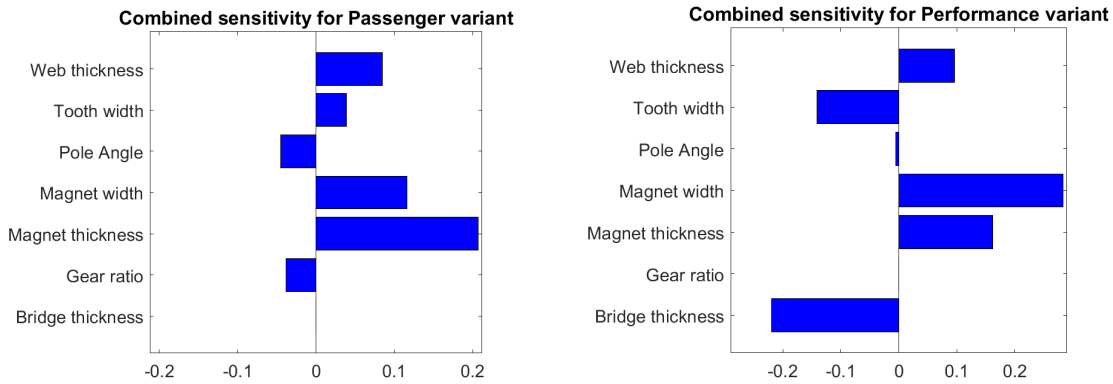

Figure 4.23: Combined Sensitivity of design parameters

Observing the Figure 4.23 we get an understanding of the parameter interactions and their cumulative effects on the powertrains's desired performance characteristics. This approach enables us to see the actual dependence of the powertrain as a whole on the particular design parameter for our specific requirement. With the insights gained from this combined sensitivity analysis, we can rank the sensitivity of the parameters:

For the Passenger variant,

1. Magnet thickness
2. Magnet width
3. Web thickness
4. Pole angle
5. Tooth width
6. Gear ratio
7. Bridge thickness

For the Performance variant,

1. Magnet width
2. Bridge thickness
3. Magnet thickness
4. Tooth width
5. Web thickness

6. Pole angle
7. Gear ratio

We can observe that the parameters, magnet thickness and magnet width have high rankings despite having lower effects on the individual outputs when compared to that of tooth width; this occurs as one focus of the optimization is the weight of the permanent magnets in the rotor, which are affected only by 'magnet width' and 'magnet thickness'. The gear ratio, which greatly affects the acceleration time, a key factor in the Performance variant, has a lower ranking as the aim of the optimization was not to reduce the acceleration time but was to ensure it met the target.

4.7 Optimization

The optimization process was based on prediction outputs of the full-factorial parameter combinations. First, the parameters combinations that do not meet the vehicle (and motor) performance targets like peak torque, peak power and acceleration time were filtered out. Then the cost for all the other parameter combinations was calculated as defined in the following section. The parameter combination with the least cost is the optimized parameters for the specific vehicle application.

4.7.1 Cost function

Cost function for Passenger variant

The function defined in Equation 4.16 below is the cost function for the optimization of parameters for the Passenger variant. Since the motor is being optimized for city driving, the cost function aims to optimize the WLTC cycle efficiency. It is crucial to define the right terms in the cost function to achieve this objective. A comprehensive analysis was conducted using simulated data to understand various performance characteristics of the motor and to select specific terms to optimize the WLTC cycle efficiency.

Analysis of the simulation data (training dataset) indicates that utilizing a lower volume of magnet can be associated with higher WLTC efficiency. This gives us an insight that reducing the magnet weight used in the motor can possibly lead to better WLTC efficiency. Similar observations can also be inferred from the sensitivity coefficients shown in Figure 4.22. Minimizing the volume of magnet used would also reduce the overall weight of the motor and hence defining the cost function such that the WLTC efficiency is maximized and the magnet weight is minimized is in the best interest of designing an optimized motor for the Passenger variant. Similar analysis was conducted on torque ripple, and it was observed that the amount of magnet used has no significant effect on the torque ripple, and the same can be inferred from the sensitivity coefficients shown in Figure 4.21 (b). Further, the sensitivity coefficients for WLTC cycle efficiency and torque ripple indicate that minimizing torque ripple would also increase the WLTC efficiency. Therefore, the cost function

is defined such that it aims to maximize WLTC cycle efficiency while minimizing torque ripple and magnet weight.

$$\text{Cost}_{\text{Passenger}} = 0.4 \times (1 - \eta_{\text{WLTC}}) + 0.2 \times T_{\text{Ripple}} + 0.4 \times M_w \tag{4.16}$$

The weights given for the cost function determine how the parameters are optimized with respect to these specific performance outputs. It is crucial to choose the right weights to achieve the objective.

1. WLTC cycle efficiency: Weight = 0.4

   For Passenger variant, WLTC cycle efficiency is considered as the most important optimization objective in this study. A higher efficiency leads to lower energy losses and reduces operating costs by augmenting the range of the car, which is a crucial factor for a passenger vehicle. Therefore, a weight of 0.4 was assigned to WLTC cycle efficiency in the cost function and the weights for other terms were assigned according to their relative importance and based on the analysis discussed above.

2. Torque ripple: Weight = 0.2

   While torque ripple is not given high importance it causes vibration, noise, and increased stress on mechanical components. Which will affect the lifetime of components in the powertrain. Hence it is beneficial to lower the torque ripple as much as possible. A weight of 0.2 was assigned to torque ripple accordingly.

3. Magnet weight: Weight = 0.4

   The magnet weight is crucial in determining the overall cost (price) of the PMSM. Additionally, as observed from the sensitivity analysis in Section 4.6.1, minimizing magnet weight used would result in higher WLTC cycle efficiency. Hence a weight of 0.4 was assigned emphasizing the importance of minimizing magnet weight, which can help reduce material costs and potentially improve the WLTC cycle efficiency.

Cost function for Performance Variant

The equation defined below is the cost function for the optimization of the parameters for the Performance variant. The cost function aims to maximize rated efficiency while minimizing torque ripple and magnet weight.

$$\text{Cost}_{\text{Performance}} = 0.4 \times (1 - \eta_{\text{Rated}}) + 0.4 \times T_{\text{Ripple}} + 0.2 \times M_w \tag{4.17}$$

Here's a breakdown of each weight and its justification:

1. Rated efficiency: Weight = 0.4

Efficiency is not a focus for optimization in a performance vehicle, but it is still considered with a weight of 0.4, as the vehicle will still be utilized for passenger use and needs to be efficient for city driving. A higher efficiency results in lower energy losses and reduced operating costs, augmenting the range of the car, which is crucial for a passenger vehicle.

2. Torque ripple: Weight = 0.4

   Torque ripple refers to the variation or fluctuation in the motor's torque output during operation. Excessive torque ripple causes vibration, noise, and increased stress on mechanical components. Since the motor is being used commercially and for passenger use, and operated at high speeds, optimizing these parameters plays a crucial role in vehicle ergonomics and performance. Thus, assigning a weight to torque ripple of 0.4 in the cost function emphasizes the importance of minimizing torque fluctuations to ensure smoother operation and improved overall performance.

3. Magnet weight: Weight = 0.2

   The magnet weight is crucial in determining the material cost and manufacturing complexity of the motor. By assigning a high weight, the cost function emphasizes the importance of minimizing magnet weight, which can help reduce material costs and potentially simplify the motor's design and manufacturing process.

In summary, the weights assigned to each term in the cost function reflect their respective importance and impact on the overall cost of the motor system. The cost function aims to maximize efficiency and minimize both torque ripple, and magnet weight, thereby promoting cost-effective motor designs with desirable performance characteristics. Despite this cost function being utilized to optimise a vehicle with performance focus, the peak torque, peak power or time to accelerate are not being maximised/minimized as the goal of this optimisation was to just ensure the vehicle met the required performance targets while being efficient. All the combinations of parameters obtained from the full factorial are processed in a way such that all the combinations of parameters resulting in a torque, power or acceleration time which do not meet the requirement are filtered out. Maximizing the torque will result in lower acceleration times but the vehicle despite being a performance car is not a formula 1 car but a high performance passenger car. Hence there is no need to further maximize the torque and other performance properties.

4.8 Vehicle model

In this study vehicle powertrain is modelled in GT-Suite, a simulation software that uses modular approach to system modelling. Individual components of a powertrain are defined and connected to each other such that the connections represent the

flow of energy or signals within the powertrain. The components defined are self-contained models that simulate the physical behavior of the component; hence these components contain sub-models that require physical principles, empirical data, or mathematical models to simulate the behavior. Figure 4.24 shows the FWD powertrain modelled in GT-Suite which was used for simulating the powertrain for Passenger variant. A similar RWD powertrain model was used for Performance variant.

For this study, the motor is modelled using `'MotorGeneratorMap'` component that requires motor performance maps as input maps and look-up tables. Performance maps like electromechanical efficiency and torque-speed curve are extracted from Motor-CAD simulations and are used as inputs to GT-Suite model. Thermal effects on performance of the PMSM were ignored in this study. The control aspect of powertrain was achieved by using the `'VehDriverAdvanced'` component. This component simulates a realistic driver behaviour with advanced settings that can be chosen appropriately for complex driving scenarios. However, in this study simple driving scenarios were simulated and hence the driver dimensionality was set to `'longitudinal'` and the driving mode was set to `'speed targeting'`. Based on the current speed and the desired speed of the vehicle, required acceleration is calculated and torque is requested from the motor accordingly.

A `'look ahead time'` for speed targeting can be set to ensure that the calculated acceleration is smooth, this attribute is set to 0.1 sec.

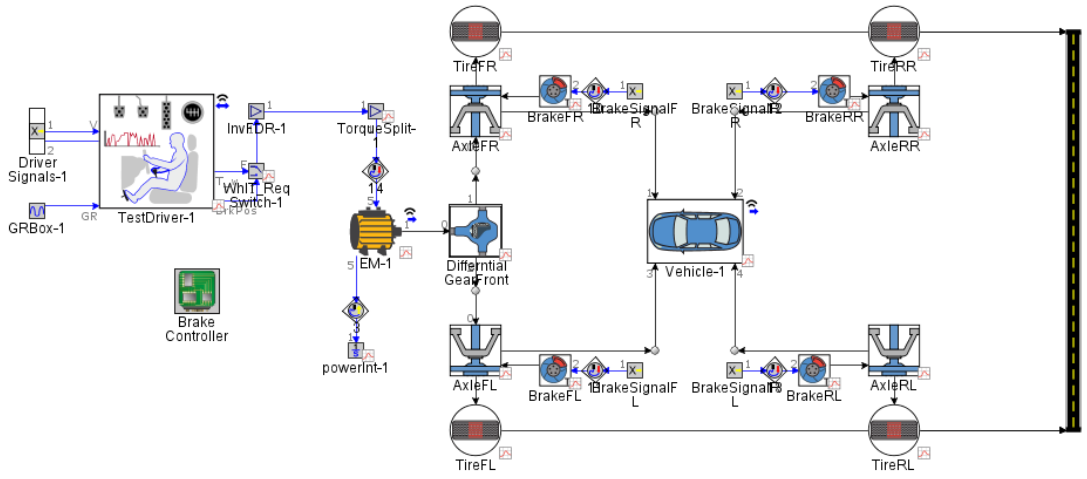

Figure 4.24: Powertrain model in GT-Suite for Passenger variant (FWD)

Two test scenarios were defined in case setup which were used to evaluate the performance of the optimized motor with respect to the baseline motor. An acceleration test where the time taken for vehicle to accelerate 0-100kmph was tested and a WLTC cycle for Passenger variant was simulated to compare the overall cycle efficiency.

5
Results

In this section we present a comprehensive analysis of the results obtained from the optimization methodology incorporated in this study. First, the optimized motor models were designed and simulated in Motor-CAD and were compared with the respective baseline motor models. The performance maps of optimized motor models were then extracted and provided as inputs to the GT-Suite powertrain models to evaluate the vehicle performance for the two defined test cases, i.e. acceleration test and WLTC cycle test.

5.1 Passenger variant

Using the regression model and the cost function defined in Section 4.7.1, the optimized parameters as shown in the below Table 5.1 are predicted to optimize the WLTC cycle efficiency, torque ripple, and magnet weight of the motor. From the parameters 'Magnet width' and 'Magnet thickness' it can be observed that the volume of the permanent magnets used is slightly reduced in the optimized motor. Furthermore, the gear ratio is increased which results in reduced accelration time according to the sensitivity analysis, Section 4.6.1.

Table 5.1: Baseline and optimized parameters for Passenger variant

Parameter	**Unit**	**Baseline**	**Optimized**
Pole angle	deg	130	140
Magnet width	mm	16	16.57
Magnet thickness	mm	5	4
Bridge thickness	mm	2	2.5
Web thickness	mm	2	2
Tooth width	mm	4.15	5.5
Gear ratio	-	9.74	10.05

The predicted performance outputs of the optimized parameters were compared to the performance outputs of the baseline parameters and are tabulated below, Table 5.2. The error in prediction is given in the form of percentage error with respect to simulated values. Most of the predictions made by regression model are accurate up to 1.27% with an exception in torque ripple, which showed a percentage error of 22.59%. The error in prediction of torque ripple is considerably huge to confidently use the torque ripple model for optimization and further methods to improve the

prediction accuracy needs to be investigated. `NOTE:` The torque ripple shown here is the torque ripple at rated operating point.

Table 5.2: Prediction error of regression model for the optimized motor outputs

Output	Unit	Predicted	Simulated	Error (%)
Peak torque	N-m	349.33	350	-0.19
Peak power	kW	143.7	141.9	1.27
Base speed	rpm	3582	3606	-0.66
Torque ripple	%	10.58	8.63	22.59
Rated efficiency	%	96.11	96.08	0.03
Cycle efficiency (WLTC)	%	94.87	94.94	-0.07
Acceleration time (0-100kmph)	s	7.49	7.37	0.02

Motor-CAD simulation

The torque-speed and power-speed characteristics of the optimized motor are shown in Figure 5.1 and Figure 5.2 respectively. The peak torque achieved with the optimized design is 350 Nm and the peak power is 141.9 kW. The base speed of the motor is 3606 RPM and the rated power is 130.8 kW. While the peak torque shows considerably improvement compared to the baseline motor, there is no considerable drop in the peak power and rated power of the motor. The base speed was reduced by $\sim$ 700 RPM, however the regression model predicts that this drop in base speed does not affect the time required to accelerate (0-100 kmph) since it is compensated by increase in peak torque. Overall, the torque-speed and power-speed curves for the optimized motor demonstrate that powertrain requirements initially derived, Table 3.1, are met.

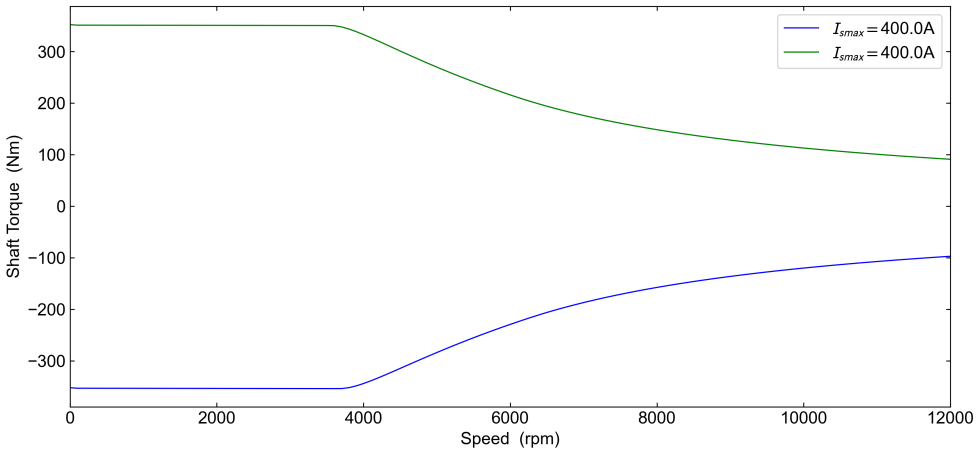

Figure 5.1: Torque-speed curve for optimized motor model for Passenger variant

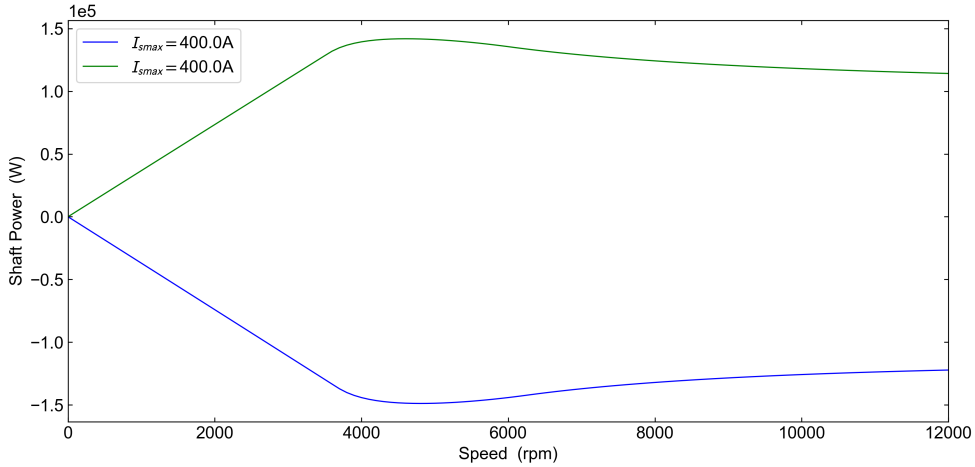

Figure 5.2: Power-speed curve for optimized motor model for Passenger variant

The efficiency map, Figure 5.3, shows that the optimized motor is as efficient as the baseline motor with slight improvement in the high-speed region. It can be observed that the region of high efficiency (efficiency $\geq 98\%$) has increased and this is noticeable at 10000 rpm. This can be observed more clearly in Figure A.2.

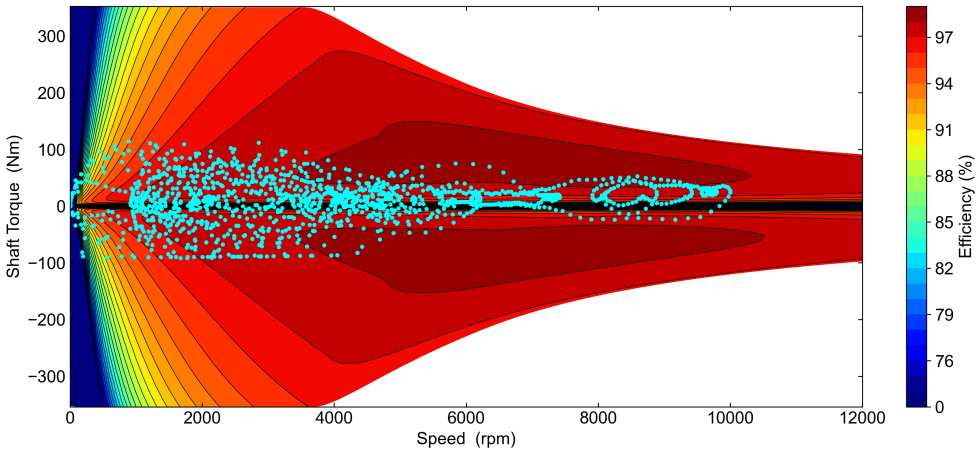

Figure 5.3: Efficiency map of the optimized motor for passenger variant

An areal analysis of efficiency map shows that the total map area has increased significantly, Figure A.1 and Figure A.2. And similar to the baseline motor, about 77% of the map area has an efficiency greater than 95%. Table 5.3 shows the areal analysis of the efficiency maps for both baseline and optimized motor. The percentage of map area above a certain efficiency is tabulated, and the delta between baseline and optimized is calculated in terms of percentage change. It can be observed that the region with efficiency $\geq 98\%$ shows significant increase, while there is a negligible decrease in regions with efficiency $< 98\%$.

Table 5.3: Areal analysis of efficiency map

Efficiency above (≥)	Baseline	Optimized	Delta (%)
98	14.67	17.69	20.58
97	55.34	55.11	-0.42
96	70.82	70.58	-0.34
95	77.81	77.56	-0.32
90	89.90	89.78	-0.13
85	93.55	93.46	-0.09

The efficiency comparison map, by taking the difference of the efficiency at each point in the efficiency map, is plotted in Figure 5.4 to identify the region with positive and negative delta with respect to the baseline efficiency. The efficiency comparison map shows that most of the WLTC operating points, marked in cyan, lie in the region with a positive delta in efficiency. The observed delta in this region is about +0.0 to +1.6, though the delta is not huge a slight increase in WLTC cycle efficiency can be observed. The point-to-point average efficiency of WLTC cycle has slightly increased to 94.94% when compared to the baseline (94.66%). There are regions with a negative delta in efficiency, which is predominant in post field weakening region, which is more evident at relatively higher speeds and at maximum limiting torque. For a passenger car designed for city driving cycles, this negative delta region has almost no impact in terms of cycle efficiency. Further, the extended high efficiency region (efficiency ≥ 98%) at 10000 RPM is likely to improve the highway cruising performance of the motor.

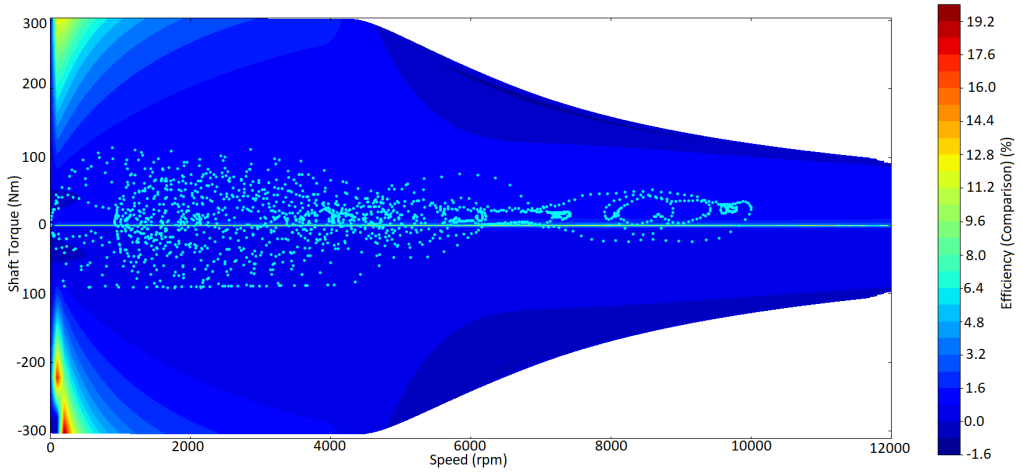

Figure 5.4: Efficiency comparison map

Figure 5.5 compares the torque ripple of the baseline and the optimized motor at rated operating point. It can be observed that the average torque of the optimized motor is higher and has a very low torque ripple when compared to that of the baseline design, the torque ripple is reduced by 70%. `NOTE:` The torque ripple shown here is the torque ripple at rated operating point.

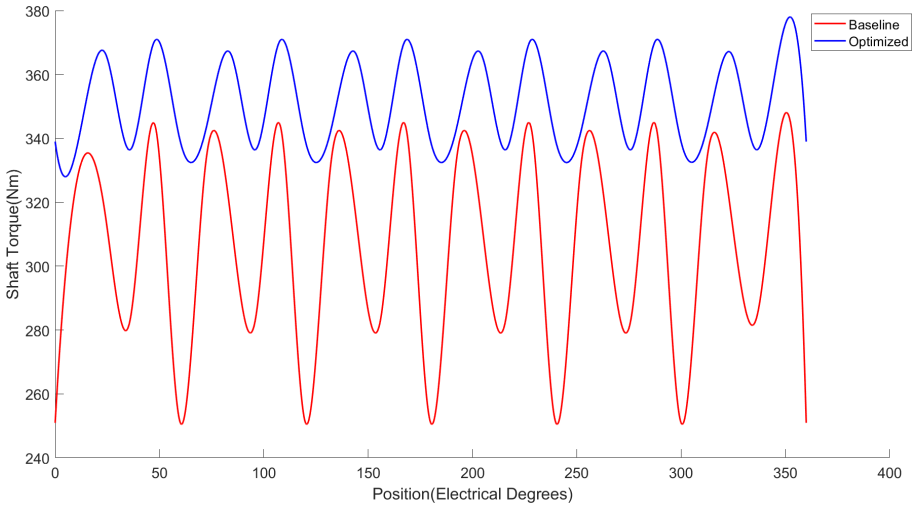

Figure 5.5: Torque ripple (at rated operating point) comparison for baseline and optimized motor

Vehicle simulation

The total loss of the motor on WLTC cycle is shown in Figure 5.6. The total loss includes copper, iron, and magnet losses. The mechanical losses were ignored in this study since the main focus was on electromagnetic performance of motor. The optimized motor has an accumulated loss of 492 kJ which slightly lower than that of the baseline motor (522 kJ). The electrical input energy required to complete the WLTC cycle is approximately the same for both optimized and baseline motor, while the optimized motor requires slightly less energy (3.731 kWh) when compared to the baseline motor (3.735 kWh).

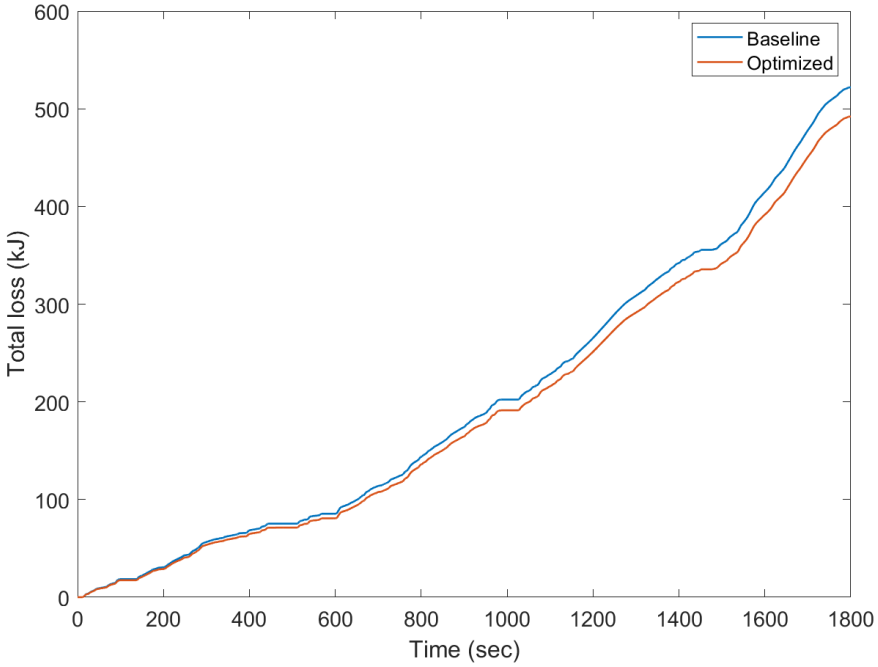

Figure 5.6: Total energy loss of the motor on WLTC cycle

The acceleration test for the baseline motor and optimized motor for the Passenger variant is shown in Figure 5.7. The baseline motor is able to achieve an acceleration time of 7.75 sec, which does not meet the acceleration targets derived Section 4.1. Whereas the optimized motor is able to achieve an acceleration time of 7.37 sec, which meets the acceleration target.

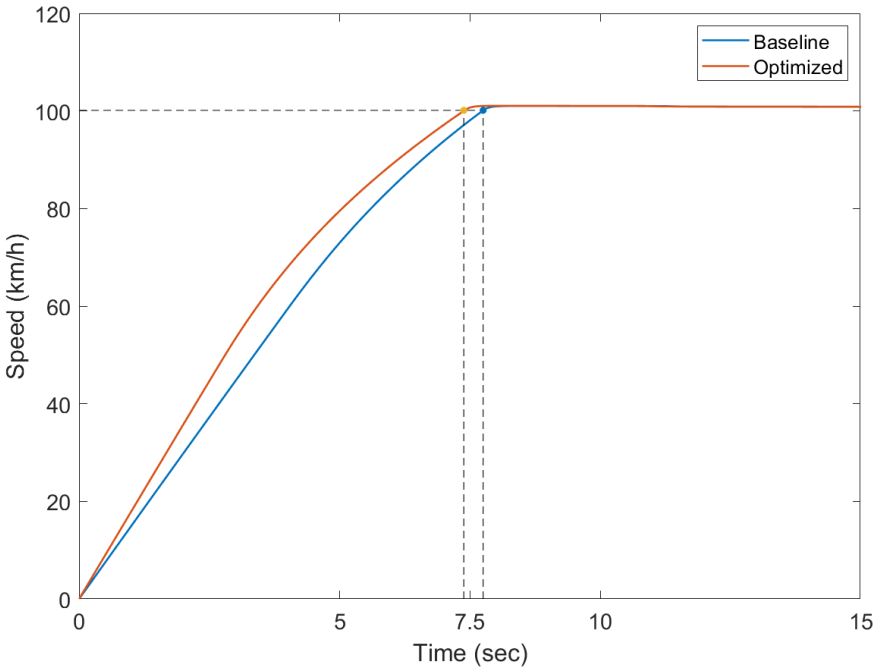

Figure 5.7: Acceleration test for Passenger variant

Overall comparison

The overall performance of the baseline and optimized motors is compared in Table 5.4. The improvement in performance is calculated in terms of percentage change with respect to the baseline. While all the objectives of the cost function are met, certain performance characteristics like peak power, base speed, and rated efficiency have dropped. But since the focus of optimization was with respect to a passenger vehicle application, the drop in these outputs is ignored. Furthermore, all the initial powertrain requirement defined for the Passenger variant have been met. `NOTE:` The torque ripple shown here is the torque ripple at rated operating point.

Table 5.4: Comparison of performance outputs for baseline and optimized parameters for Passenger variant

Output	Unit	Baseline	Optimized	Delta (%)
Peak torque	N-m	305	350	14.75
Peak power	kW	145.5	141.9	-2.47
Torque ripple	N-m	28.77	8.63	-70
Rated efficiency	%	96.17	96.08	-0.09
WLTC cycle efficiency	%	94.66	94.94	0.29
Magnet weight	kg	2.205	1.958	-11.2
Acceleration time (0-100 kmph)	s	7.75	7.37	-4.9

5.2 Performance Variant

The prediction model with the aid of the cost function in 4.7.1 was able to simulate and generate an output in-terms of a parameter combination which should yield the required performance requirement as calculated in Section 4.1. The motor was redesigned using the optimised parameters and is simulated on Motor CAD to verify if the results from the prediction model resonates with the simulated results and to what extent the baseline model is optimized.

Table 5.5: Baseline and optimized design parameters of PMSM (and gear ratio)

Parameter	Unit	Baseline	Optimized
Pole angle	deg	130	130
Magnet width	mm	22	23
Magnet thickness	mm	7.57	6.71
Bridge thickness	mm	2	3.14
Web thickness	mm	5.8	2
Tooth width	mm	4.78	5.5
Gear ratio	-	8.74	11.24

The output of the optimised motor predicted by the algorithm and the actual value obtained by manually simulating the motor are compared in the table 5.6. The error in prediction is depicted in the form of percentage error with respect to simulated values. All of the predictions by regression model are accurate up to 2.39%. From this we can observe that the error of the prediction model is low. Despite using a similar prediction technique and a similar training set as the passenger variant, this model shows a better accuracy. The predicted parameter combination or a combination very similar to this could have been fed in as a part of the training set which could explain the lower prediction error. `NOTE:` The torque ripple shown here is the torque ripple at rated operating point.

Table 5.6: Prediction error of regression model for the optimized motor outputs

Output	Unit	Predicted	Simulated	Error (%)
Peak torque	Nm	535.3	534	0.24
Peak power	kW	251.9	250.7	0.47
Base speed	rpm	4226	4248	-0.51
Torque ripple	%	13.95	13.62	2.39
Rated efficiency	%	96.9	96.9	0
Acceleration time (0-100kmph)	s	5.05	5.0	0.98

Motor-CAD simulation

From analysing the Torque-Speed and Power-Speed curves depicted in 5.9 and 5.8 of the PMSM, it can be observed that the torque of the optimised motor is higher than that of the baseline where as the peak power has slightly lower than the baseline, this is due to the reduction in base speed which is the region where field weakening occurs, this occurred as the torque was increased to meet the acceleration target. Despite this both the torque and power of the motor satisfy the specified requirements. This suggests that the designed PMSM is suitable for this particular use case.

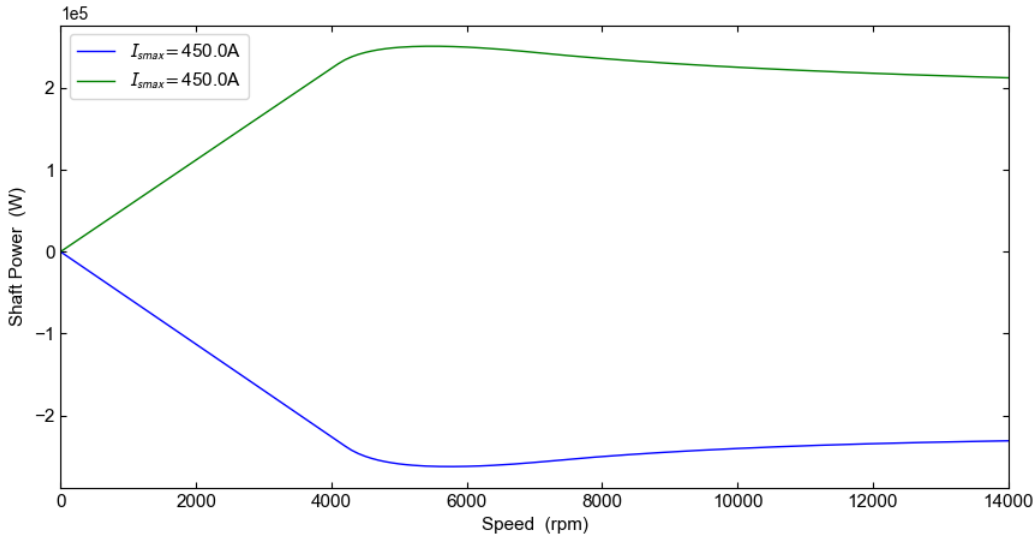

Figure 5.8: Power-Speed curve of the optimized motor

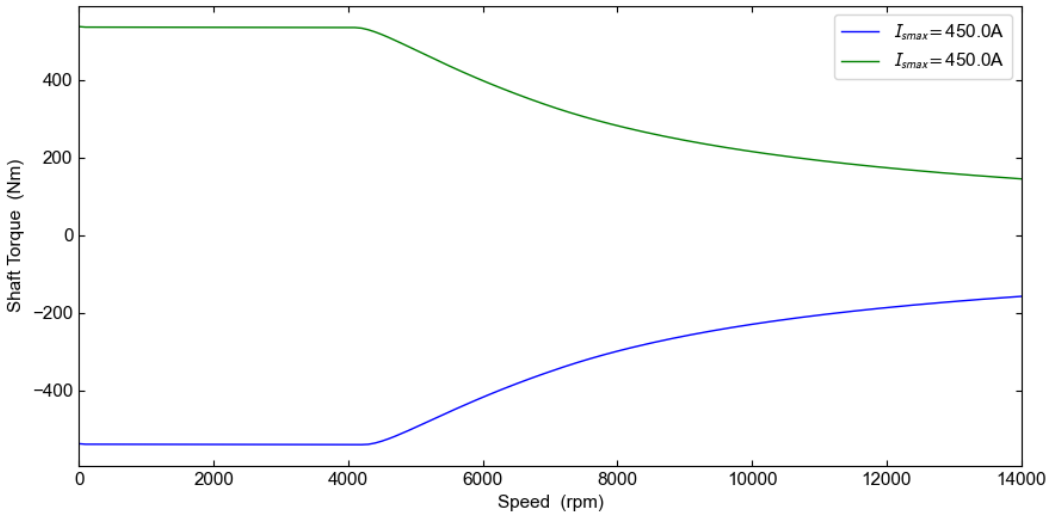

Figure 5.9: Torque-Speed curve of the optimized motor

The efficiency map of the optimized PMSM in 5.10 reveals large regions of high efficiency across various operating points, affirming its efficient performance characteristics. For the use-case of a performance car, efficiency is not the main focus but a suitable weight was given to ensure the vehicle has an acceptable efficiency for passenger use. Examining the efficiency map, it becomes evident that the PMSM excels in maintaining high efficiency exceeding 95% in regions of high torque and high speed which are common operating points for a performance vehicle.

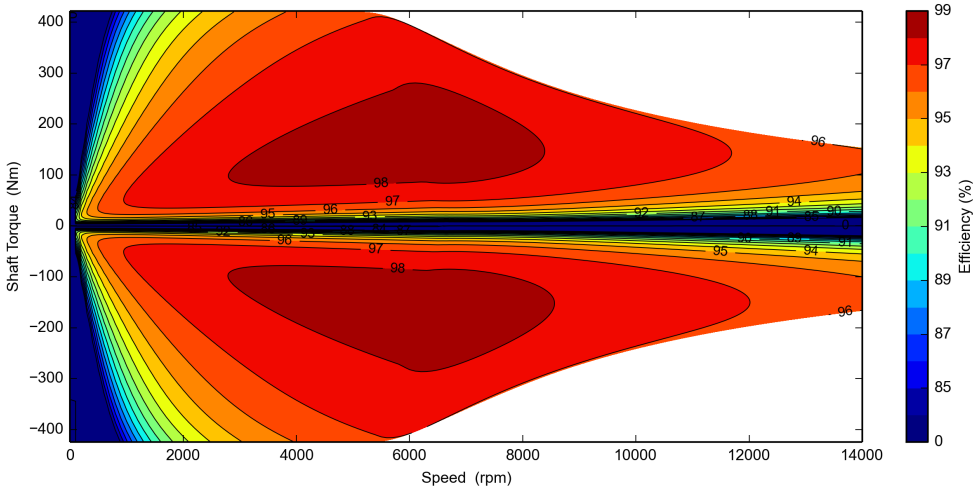

Figure 5.10: Efficiency map of the optimized motor

From the figure 5.11 which depicts the variation of torque output vs. Electrical degree, it is evident that the baseline and optimized systems exhibit distinct characteristics in terms of torque ripple. The torque output of the optimized motor demonstrates a significant reduction(52%) in torque ripple compared to the baseline

model. The torque ripple of the optimized motor measures around 14% of the average torque value. The minimized torque ripple in the optimized system results in a more even output of torque which is highly desired for this application and it further leads to improved efficiency, reduced vibrations, and enhanced overall system stability.

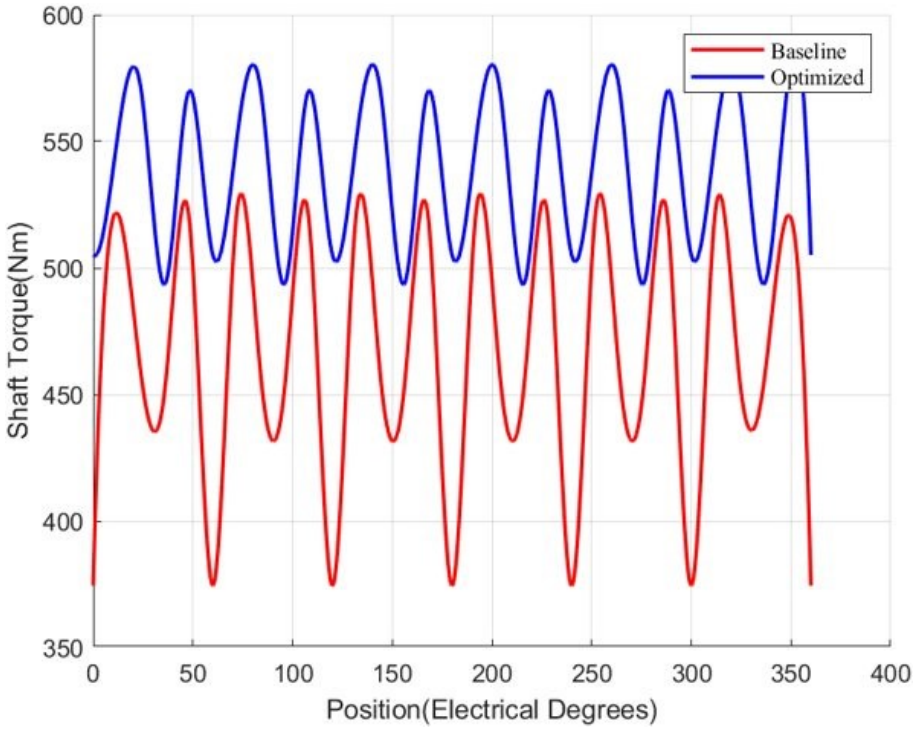

Figure 5.11: Torque Ripple of the optimized motor

Vehicle simulation

The figure 5.12 depicts the vehicle's acceleration performance. The two curves depict the acceleration profile of the vehicle with and without tyre slip consideration. We can observe that the acceleration curve in blue which does not consider tyre slip reaches 100 km/hr much earlier compared to the red curve which is the vehicle model considering tyre slipping. In this thesis, we have not considered the effects of tyre slipping while optimizing for acceleration time. We can see that the vehicle reaches 100 km/hr in 5 seconds which is well below the pre-defined target.

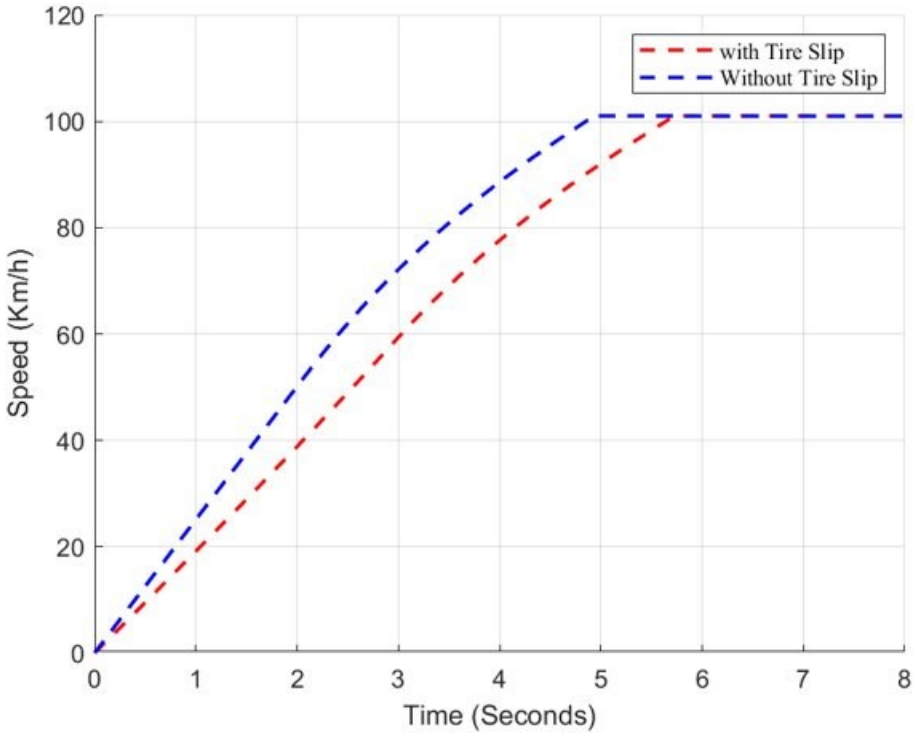

Figure 5.12: Acceleration profile for the optimized motor

Overall comparison

The overall performance of the baseline and optimized motors for the performance variant is compared in Table 5.7. The change in the performance is depicted in terms of delta percentage. We can observe that the optimised motor meets all the performance requirements of the vehicle while having significantly lower torque ripple(a reduction of 52%) with respect to the baseline. This was achieved while simultaneously reducing the volume of magnets used thereby reducing manufacturing costs and maintaining a high efficiency. While all the objectives of the optimisation have been met, there was a slight decrease in peak power which is not a concern as the peak power requirement is still met. `NOTE:` The torque ripple shown here is the torque ripple at rated operating point.

Table 5.7: Performance comparison between the Baseline and optimized motor)

Output	Unit	Baseline	Optimized	Delta (%)
Peak Torque	N-m	512	534	4.26
Peak Power	W	252.4	250.7	-0.79
Torque Ripple	N-m	28.4	13.62	-52
Rated Efficiency	%	96.8	96.9	0.1
Magnet Weight	kg	4.40	4.12	-6.2
Acceleration Time (0-100 kmph)	s	5.66	5.0	-11.62

6
Conclusion

The study aimed to analyze and optimize the design parameters of EDU, with a specific focus on the electric motor. Design parameters were identified through parameter study and literature survey and the effect of these parameters on performance outputs like torque, peak power, torque ripple, and efficiency was investigated. A methodology to optimize these parameters was proposed in this study, in which prediction models were built using regression modelling techniques to optimize the design parameters for specific vehicle application. Gaussian process regression model was used to optimize the design parameters since it showed higher prediction accuracy. Linear regression coefficients were used to investigate the first-order sensitivity of the design parameters and it was found that Tw, Lm and Wb have the highest influence for most of the outputs. A combined sensitivity, defined for specific vehicle application, was investigated and it was found that for Passenger variant with efficiency (WLTC) focus and it was concluded that the parameters can be ranked as $Hm > Lm > Tj > \theta > Tw > FDR > Wb$ and for Performance variant with performance (high acceleration) focus the parameters can be ranked as $Lm > Wb > Hm > Tw > Tj > \theta > FDR$. This ranking is dependant on the optimization objective function (or cost function) defined in this study and hence the ranking is also affected by the importance given to lowering the cost of the motor by reducing the amount of permanent magnet used in the Passenger variant case; and the importance given to lowering the torque ripple for smoother high torque application in the Performance variant case.

The optimization methodology incorporated in this study proved to improve the WLTC efficiency of the Passenger variant by 0.29%, while reducing the amount of permanent magnet used by 11.2%. And the acceleration time for the Performance variant was reduced by 11.6%, while reducing the torque ripple at rated operating point by 52%. Therefore the optimization methodology proposed in this study provides framework for defining the cost function and to optimize the design parameters to meet the desired vehicle performance targets.

6.1 Limitations

- **Manufacturability:** the manufacturability of the motor with respect to the design parameters used in this study was not considered while defining the parameter levels. Though an inbuilt `'Geomerty check'` feature in MotorCAD was used for PMSM design parameters, the tolerances of the design

parameters were not validated through any practical means.

- **Rotor duct:** a rotor duct in a PMSM can significantly impact the performance. In this study, the rotor duct implemented in the design was motivated from the reference motor design specification provided by Aurobay. The placement of the rotor duct was done such that the duct is always in between the V-shaped magnets, Figure 4.9. This placement was ensured when geometrical parameters were varied, but the effect of the duct placement on performance outputs considered in this study was not investigated.
- **Current input:** an ideal `'Sine'` current wave form was used for the simulation of PMSM performance, whereas in practical applications the current wave form is generated through pulse width modulation (PWM) and this will typically result in significant increase in torque ripple and losses due to the inverter switching frequency. A `'Custom'` current input could be provided in Motor-CAD to emulate PWM current response but this was not considered since it was not within the scope of this study.
- **WLTC torque ripple:** unlike the WLTC efficiency where a point-to-point average efficiency (an output metric of `'Duty cycle'` simulation on Motor-CAD) was used to optimize the motor, a similar approach to calculate the WLTC torque ripple could not be done since this would require multiple `'EMag'` simulations (= no. of operating points) for each parameter combination and this would significantly increase the computational time required. One alternative to address this in future research would be to classify these operating points into clusters and calculate the torque ripple at the centers of these clusters to effectively calculate average torque ripple over WLTC cycle.
- **Benchmark validation:** the FEA simulations used in this study were not validated on a physical prototype and hence the validity of the results could be questioned. However, through literature survey it was found that similar FEA based optimization methods were incorporated by researchers and the validity of FEA simulations were verified by experiment with a prototype in their research [1].

6.2 Future work

For a PMSM there are multiple parameters which can be included in the study such as:

- **Stator and rotor winding configuration:** The number of turns in the stator and rotor windings, their connection pattern, and wire gauge can affect the motor's electromagnetic behavior, efficiency, and torque output.
- **Magnet strength and shape:** The strength of the permanent magnets and their shape can affect the motor's torque output, power density, and efficiency.
- **Rotor and stator lamination material and thickness:** The choice of lamination material and thickness can affect the motor's magnetic properties, core losses, and efficiency.
- **Slot and pole number:** The number of rotor poles and stator slots can affect the motor's torque production, back EMF waveform, and cogging torque.

- **Airgap length:** The airgap between the rotor and stator can affect the motor's torque production, reluctance torque, and cogging torque.

Bibliography

[1] Chen, H. and Lee, C.H., 2019. Parametric sensitivity analysis and design optimization of an interior permanent magnet synchronous motor. IEEE Access, 7, pp.159918-159929.

[2] Kim, K.C., Koo, D.H., Hong, J.P. and Lee, J., 2007. A study on the characteristics due to pole-arc to pole-pitch ratio and saliency to improve torque performance of IPMSM. IEEE Transactions on Magnetics, 43(6), pp.2516-2518.

[3] Kano, Y., 2015. Torque ripple reduction of saliency-based sensorless drive concentrated-winding IPMSM using novel flux barrier. IEEE Transactions on Industry Applications, 51(4), pp.2905-2916.

[4] Sun, X., Shi, Z., Lei, G., Guo, Y. and Zhu, J., 2019. Analysis and design optimization of a permanent magnet synchronous motor for a campus patrol electric vehicle. IEEE Transactions on Vehicular Technology, 68(11), pp.10535-10544.

[5] Ahmadi, S., Lubin, T., Vahedi, A. and Taghavi, N., 2021. Sensitivity-based optimization of interior permanent magnet synchronous motor for torque characteristic enhancement. Energies, 14(8), p.2240.

[6] Veiga, I.V.A., Zymler, R., Shayani, R.A., Viana, D.M. and Orrico, M.V.M., 2012, September. Sizing of motor and battery pack for an automotive electric vehicle given a specific route. In 2012 Sixth IEEE/PES Transmission and Distribution: Latin America Conference and Exposition (T&D-LA) (pp. 1-8). IEEE.

[7] Chin, Y.K., 2004. A permanent magnet synchronous motor for an electric vehicle-design analysis (Doctoral dissertation, Elektrotekniska system).

[8] Yılmaz, M. and Özdemir, S., 2021, October. Review of Motors used in Commercial Electric Vehicles. In Proceedings of the 5th International Mediterranean Science and Engineering Congress (IMSEC 2020), Antalya, Turkey (pp. 21-23).

[9] Agamloh, E., Von Jouanne, A. and Yokochi, A., 2020. An overview of electric machine trends in modern electric vehicles. Machines, 8(2), p.20.

[10] Rasmussen, C. E. and C. K. I. Williams, 2005. Gaussian Processes for Machine Learning. MIT Press, Cambridge, Massachusetts.

[11] Schulz, E., Speekenbrink, M. and Krause, A., 2018. A tutorial on Gaussian process regression: Modelling, exploring, and exploiting functions. Journal of Mathematical Psychology, 85, pp.1-16.

[12] Mishra, A., Agarwal, P. and Srivastava, S.P., 2014. A comprehensive analysis and implementation of vector control of permanent magnet synchronous motor. International Journal of Power and Energy Conversion, 5(1), pp.1-23.

[13] Kacker, R.N., Lagergren, E.S. and Filliben, J.J., 1991. Taguchi's orthogonal arrays are classical designs of experiments. Journal of research of the National Institute of Standards and Technology, 96(5), p.577.

[14] Dumouchel, W. and O'brien, F., 1989, April. Integrating a robust option into a multiple regression computing environment. In Computer science and statistics: Proceedings of the 21st symposium on the interface (pp. 297-302). Alexandria, VA: American Statistical Association.

[15] Holland, P.W. and Welsch, R.E., 1977. Robust regression using iteratively reweighted least-squares. Communications in Statistics-theory and Methods, 6(9), pp.813-827.

[16] Huber, P.J., Robust Statistics. 1981: Hoboken.

[17] Street, J.O., Carroll, R.J. and Ruppert, D., 1988. A note on computing robust regression estimates via iteratively reweighted least squares. The American Statistician, 42(2), pp.152-154.

A

Appendix 1

A.1 Design of experiments

Table A.1: Orthogonal array of experiments

Sim. no.	P_1	P_2	P_3	P_4	P_5	P_6	P_7
1	0	0	0	0	0	0	0
2	0	1	1	1	1	1	1
3	0	2	2	2	2	2	2
4	0	3	3	3	3	3	3
5	0	4	4	4	4	4	4
6	0	5	5	5	5	5	5
7	0	6	6	6	6	6	6
8	0	7	7	7	7	7	7
9	1	0	1	2	3	4	5
10	1	1	2	3	4	5	6
11	1	2	3	4	5	6	7
12	1	3	4	5	6	7	0
13	1	4	5	6	7	0	1
14	1	5	6	7	0	1	2
15	1	6	7	0	1	2	3
16	1	7	0	1	2	3	4
17	2	0	2	4	6	0	2
18	2	1	3	5	7	1	3
19	2	2	4	6	0	2	4
20	2	3	5	7	1	3	5
21	2	4	6	0	2	4	6
22	2	5	7	1	3	5	7
23	2	6	0	2	4	6	0
24	2	7	1	3	5	7	1
25	3	0	3	6	1	4	7
26	3	1	4	7	2	5	0
27	3	2	5	0	3	6	1
28	3	3	6	1	4	7	2
29	3	4	7	2	5	0	3
30	3	5	0	3	6	1	4
31	3	6	1	4	7	2	5

Continuation of Table A.2							
Sim. no.	P_1	P_2	P_3	P_4	P_5	P_6	P_7
32	3	7	2	5	0	3	6
33	4	0	4	0	4	0	4
34	4	1	5	1	5	1	5
35	4	2	6	2	6	2	6
36	4	3	7	3	7	3	7
37	4	4	0	4	0	4	0
38	4	5	1	5	1	5	1
39	4	6	2	6	2	6	2
40	4	7	3	7	3	7	3
41	5	0	5	2	7	4	1
42	5	1	6	3	0	5	2
43	5	2	7	4	1	6	3
44	5	3	0	5	2	7	4
45	5	4	1	6	3	0	5
46	5	5	2	7	4	1	6
47	5	6	3	1	5	2	7
48	5	7	4	2	6	3	0
49	6	0	6	4	2	0	6
50	6	1	7	5	3	1	7
51	6	2	0	6	4	2	0
52	6	3	1	7	5	3	1
53	6	4	2	0	6	4	2
54	6	5	3	1	7	5	3
55	6	6	4	2	0	6	4
56	6	7	5	3	1	7	5
57	7	0	7	6	5	4	3
58	7	1	0	7	6	5	4
59	7	2	1	0	7	6	5
60	7	3	2	1	0	7	6
61	7	4	3	2	1	0	7
62	7	5	4	3	2	1	0
63	7	6	5	4	3	2	1
64	7	7	6	5	4	3	2

Table A.2: Random-walk parameter combinations for Passenger variant

Sim. no.	θ	**Lm**	**Hm**	**Wb**	**Tj**	**Tw**	**FDR**
1	108	14	7.5	1.8	2.6	5.3	6.55
2	132	16	5.9	4.2	2.2	4.6	6.55
3	111	13	6.4	3.9	3.8	4.9	7.05
4	131	14	5.4	4.2	5.4	3.3	7.55
5	120	16	4.4	3.5	5.8	3.2	6.55
6	106	16	6.5	1.4	4.9	5	10.05
7	99	14	5.4	1.3	6.3	3.8	8.55

Continuation of Table A.2							
Sim. no.	***θ***	**Lm**	**Hm**	**Wb**	**Tj**	**Tw**	**FDR**
8	97	14	5.6	3	4.9	4.4	10.05
9	125	18	5.2	3	5.3	3.6	10,05
10	127	14	4.3	1.1	5.7	4.4	8.05
11	128	18	5.6	2.1	2	4	8.05
12	131	15	6.8	2	4.4	4.8	9.05
13	98	15	4.7	2.8	6.1	5.1	9.55
14	109	15	5.6	2.1	2.8	4.5	8.05
15	129	16	4.7	2.1	6.4	3.7	8.55

Table A.3: Parameters and levels for Performance variant

Parameter		**Unit**	**0**	**1**	**2**	**3**	**4**	**5**	**6**	**7**
P_1	θ	deg	95	100	105	110	115	120.1	125	130
P_2	Lm	mm	16	17	18	19	20	21	22	23
P_3	Hm	mm	5	5.4	5.8	6.3	6.7	7.1	7.5	8
P_4	Wb	mm	2	2.6	3.3	3.9	4.6	5.2	5.9	6.5
P_5	Tj	mm	2	2.6	3.1	3.7	4.3	4.8	5.4	6
P_6	Tw	mm	3	3.4	3.7	4.1	4.5	4.8	5.1	5.5
P_7	FDR	-	7.74	8.24	8.74	9.24	9.74	10.24	10.74	11.24

Table A.4: Random-walk parameter combinations for Performance variant

Sim. no.	***θ***	**Lm**	**Hm**	**Wb**	**Tj**	**Tw**	**FDR**
1	105	20	5.6	3.0	3.9	6.4	116
2	114	19	7.5	3.8	5.4	6.0	117
3	101	20	6.7	3.6	4.8	4.2	109
4	97	19	5.2	3.0	4.5	3.8	110
5	123	17	6.6	5.5	3.4	4.0	123
6	118	18	5.5	2.7	3.4	5.2	126
7	117	19	7.0	2.1	3.1	3.1	123
8	115	18	5.4	5.8	5.2	4.8	120
9	96	21	6.3	4.7	4.5	2.6	104
10	107	18	7.7	3.9	4.8	2.9	111
11	129	17	7.4	5.9	3.1	2.4	124
12	97	17	5.2	3.6	5.4	6.3	109
13	126	16	7.9	2.3	5.1	2.3	126
14	126	21	7.0	3.4	3.5	4.7	127
15	96	18	7.2	2.7	3.5	5.3	104

A.2 Regression models for Passenger variant

1. Torque of PMSM at rated operating point (peak torque):

$$\begin{aligned}\hat{y}_{torque} = {} & 0.0156 \cdot \hat{x}_{\theta} + 0.2409 \cdot \hat{x}_{Lm} + 0.0665 \cdot \hat{x}_{Hm} - 0.1719 \cdot \hat{x}_{Wb} \\ & - 0.0384 \cdot \hat{x}_{Tj} + 0.6948 \cdot \hat{x}_{Tw} + 0.1415\end{aligned} \tag{A.1}$$

2. Peak power of PMSM:

$$\begin{aligned}\hat{y}_{power,peak} = {} & 0.1118 \cdot \hat{x}_{\theta} + 0.5487 \cdot \hat{x}_{Lm} + 0.1903 \cdot \hat{x}_{Hm} - 0.3711 \cdot \hat{x}_{Wb} \\ & - 0.1228 \cdot \hat{x}_{Tj} + 0.0608 \cdot \hat{x}_{Tw} + 0.3201\end{aligned} \tag{A.2}$$

3. Acceleration time (0-100 kmph) of vehicle:

$$\begin{aligned}\hat{y}_{time,acc} = {} & -0.0612 \cdot \hat{x}_{\theta} - 0.2163 \cdot \hat{x}_{Lm} - 0.0789 \cdot \hat{x}_{Hm} + 0.1311 \cdot \hat{x}_{Wb} \\ & + 0.0394 \cdot \hat{x}_{Tj} - 0.4124 \cdot \hat{x}_{Tw} - 0.3080 \cdot \hat{x}_{FDR} + 0.7520\end{aligned} \tag{A.3}$$

4. Base speed of PMSM:

$$\begin{aligned}\hat{y}_{speed,base} = {} & 0.0177 \cdot \hat{x}_{\theta} + 0.0190 \cdot \hat{x}_{Lm} + 0.0216 \cdot \hat{x}_{Hm} - 0.0088 \cdot \hat{x}_{Wb} \\ & - 0.0281 \cdot \hat{x}_{Tj} - 0.8971 \cdot \hat{x}_{Tw} + 0.8328\end{aligned} \tag{A.4}$$

5. Airgap flux density (mean) at rated operating point:

$$\begin{aligned}\hat{y}_{FluxDensity} = {} & -0.0175 \cdot \hat{x}_{\theta} + 0.0460 \cdot \hat{x}_{Lm} + 0.0061 \cdot \hat{x}_{Hm} - 0.0623 \cdot \hat{x}_{Wb} \\ & + 0.0185 \cdot \hat{x}_{Tj} + 0.7999 \cdot \hat{x}_{Tw} + 0.1003\end{aligned} \tag{A.5}$$

6. Torque ripple of PMSM at rated operating point:

$$\begin{aligned}\hat{y}_{TorqueRipple} = {} & -0.0593 \cdot \hat{x}_{\theta} + 0.0181 \cdot \hat{x}_{Lm} - 0.0225 \cdot \hat{x}_{Hm} - 0.2479 \cdot \hat{x}_{Wb} \\ & + 0.3381 \cdot \hat{x}_{Tj} - 0.5063 \cdot \hat{x}_{Tw} + 0.6178\end{aligned} \tag{A.6}$$

7. Efficiency of PMSM at rated operating point:

$$\begin{aligned}\hat{y}_{efficiency,rated} = {} & 0.0554 \cdot \hat{x}_{\theta} + 0.4626 \cdot \hat{x}_{Lm} + 0.1532 \cdot \hat{x}_{Hm} - 0.3029 \cdot \hat{x}_{Wb} \\ & - 0.1006 \cdot \hat{x}_{Tj} + 0.1543 \cdot \hat{x}_{Tw} + 0.4594\end{aligned} \tag{A.7}$$

8. Cycle efficiency (point-to-point average) of PMSM on WLTC cycle:

$$\begin{aligned}\hat{y}_{efficiency,WLTC} = {} & -0.0622 \cdot \hat{x}_{\theta} - 0.1747 \cdot \hat{x}_{Lm} - 0.0200 \cdot \hat{x}_{Hm} + 0.1234 \cdot \hat{x}_{Wb} \\ & + 0.0377 \cdot \hat{x}_{Tj} + 0.3547 \cdot \hat{x}_{Tw} - 0.0957 \cdot \hat{x}_{FDR} + 0.6397\end{aligned} \tag{A.8}$$

A.3 Results

A.3.1 Areal analysis of efficiency map for Passenger variant

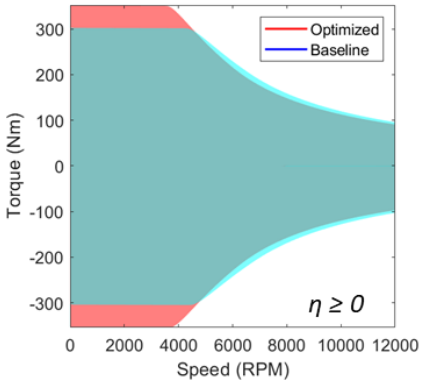

Figure A.1: Comparison of total motor map region for baseline and optimized motor for Passenger variant

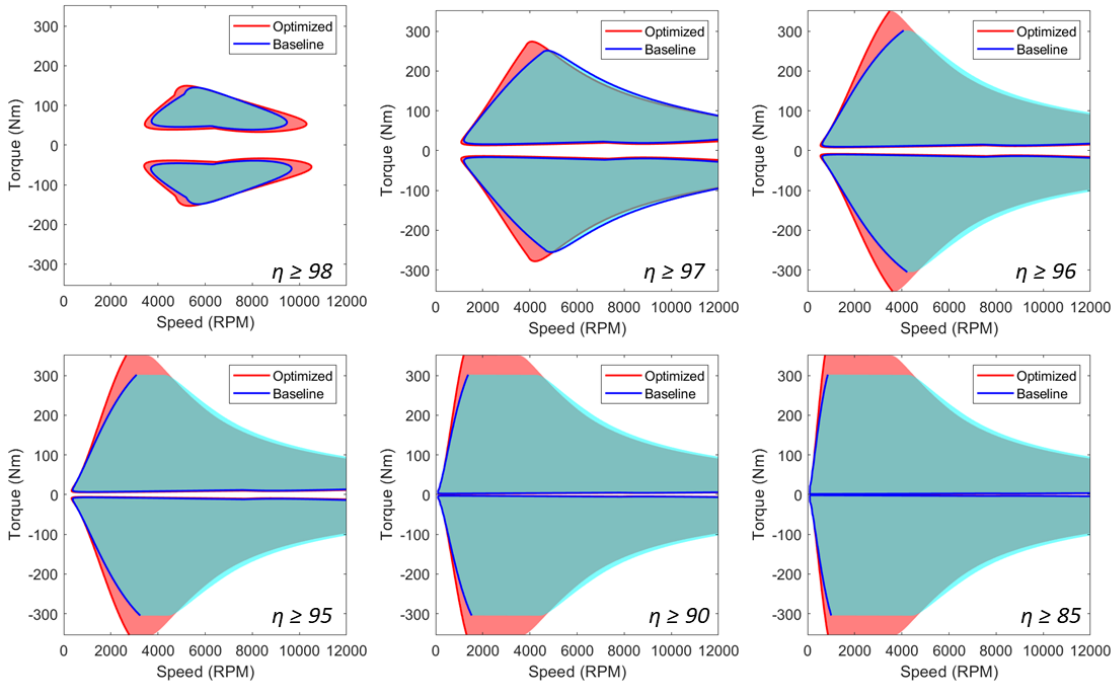

Figure A.2: Areal analysis of motor map region for baseline and optimized motor for Passenger variant

DEPARTMENT OF MECHANICS AND MARITIME SCIENCES
CHALMERS UNIVERSITY OF TECHNOLOGY
Gothenburg, Sweden
www.chalmers.se

CHALMERS
UNIVERSITY OF TECHNOLOGY